# AGE AND GEOCHEMISTRY OF BASALT-CHERT ASSOCIATIONS IN THE OPHIOLITES OF THE IZMIR-ANKARA MÉLANGE EAST OF ANKARA, TURKEY: PRELIMINARY DATA

**Valerio Bortolotti*, Marco Chiari**,✉, M. Cemal Göncüoglu***, Marta Marcucci*, Gianfranco Principi*, U. Kagan Tekin°, Emilio Saccani°°** and **Renzo Tassinari°°**

* *Dipartimento di Scienze della Terra, Università di Firenze, Italy.*
** *CNR, Istituto di Geoscienze e Georisorse, Italy.*
*** *Middle East Technical University, Geological Engineering Department, Ankara, Turkey.*
° *Hacettepe University, Geological Engineering Department, Ankara, Turkey.*
°° *Dipartimento di Fisica e Scienze della Terra, Università di Ferrara, Italy.*
✉ *Corresponding author, email: mchiari@geo.unifi.it*

**Keywords:** *Ophiolites, basalts, geochemistry, radiolarians, Triassic, Jurassic, Early Cretaceous, Izmir-Ankara Mélange. Turkey.*

ABSTRACT

In this paper, we present the preliminary data on the age of the radiolarian cherts deposited on top of basalts belonging to the Eastern Ankara Mélange (part of the Izmir-Ankara Mélange). Petrological studies on the basalts were carried out in order to constrain the tectonic setting of the studied basalt-chert sequences. Nine sections were sampled East and Northeast of Ankara and twenty seven samples were collected for biostratigraphic and geochemical analyses.

The oldest radiolarian cherts dated in the present paper are referable to the Late Triassic (Section 6: late Norian) and are associated with basaltic rocks of OIB character. OIB type volcanic rocks are also found in other sections, associated with cherts of Late Jurassic (Section 3: middle-late Oxfordian to late Kimmeridgian-early Tithonian) and Early Cretaceous (Section 1: late Valanginian to late Hauterivian) ages.

E-MORB type rocks are associated with radiolarian cherts of Cretaceous age (Section 4: middle late Barremian-early early Aptian and Section 7: Valanginian to middle Aptian-early Albian), whereas the oldest N-MORBs were found in a section of Late Jurassic age (Section 5: early-early late Tithonian). Other N-MORBs are associated with radiolarian cherts of Early Cretaceous age (Section 8: late Valanginian-early Barremian). P-MORBs type rocks were found only in a section of Middle Jurassic age (Section 2: early-middle Bajocian to late Bathonian-early Callovian age).

In this work, we document the occurrence of Late Triassic OIB-type rocks and of rocks showing different geochemical affinities (N-, E-, P-MORBs and OIB) generated within the same time span (Middle-Late Jurassic - Early Cretaceous). N-MORBs are compatible with composition of melts generated by partial melting of a depleted MORB mantle source. In contrast, OIBs are compatible with partial melting of an enriched-type mantle source. E-MORBs may have derived from mantle source slightly enriched with respect to a DMM source, whereas P-MORBs are compatible with melts generated from a mantle source significantly enriched, compared to DMM.

## INTRODUCTION

At a large scale, Anatolia can be subdivided into four main continental zones (from N to S) (see Fig. 1): 1) Rhodope Pontide Terranes (IZT in Fig. 1), 2) Sakarya Composite Terrane (SCT in Fig. 1), 3) Anatolides and Taurides (= Tauride-Anatolide Platform; ATB in Fig. 1) and 4) the SE Anatolian Autochthon. Between the Sakarya Terrane and the Anatolides (Kutahya-Bolkardag belt in the Western and Kirşehir Massif in the Central Turkey), an ophiolitic suture occurs, known as the Izmir-Ankara-Erzincan Suture Belt (IAESB), evidence of the presence of an ancient ocean basin: the Izmir-Ankara section of the Eastern Mesozoic Tethys Ocean (see Sengör and Yilmaz, 1981; Dercourt et al., 1986; Robertson et al., 1996; Dilek et al., 1999; Göncüoglu et al., 1997, 2000; 2006; 2010; Stampfli and Borel, 2002; Bortolotti and Principi, 2005; Schmid et al., 2008; Moix et al., 2008).

This ocean basin has been correlated with the Vardar Ocean of the Dinarides-Hellenides (see Sengör and Yilmaz 1981; Robertson, 2002; 2004; Okay et al., 2006). Remnants of this ocean rode onto the northern continental margin of the Anatolide Platform. They consist of: a) an accretionary prism (the "Ankara Mélange" of Bailey and McCallien, 1953, *sensu lato*) where both ophiolite and blueschist blocks coexist, b) south-verging tectonic slices or giant slide blocks of ophiolites (see Göncüoglu et al., 2000; Göncüoglu, 2011; Floyd et al., 2000), and c) imbricated slices of succession representative of a foredeep basin, where slide blocks of a) and b) were deposited. The ophiolitic slide blocks mainly consist of peridotites (harzburgites) and also gabbros, sheeted dykes, basalts and pelagic sediments (see Önen, 2003) with predominant SSZ and, subordinately, MORB and OIB affinities (see Robertson, 2000; Floyd et al., 2000, Göncüoglu et al., 2010; Parlak et al., 2012).

The detailed multidisciplinary knowledge of these ocean-derived rocks, including their regional geology, petrology, geochemistry, stratigraphy and radiolarian biostratigraphy, allows the reconstruction of the geodynamic history of the ocean from birth, to spreading phase and closure with obduction of part of its lithosphere onto the continental margin of the Anatolide Platform.

This paper intends to contribute to this complex history through the study, in the Eastern Ankara Mélange (part of the Izmir-Ankara Mélange) of the radiolarian assemblages (and hence of the ages) of the cherts deposited on top of the ophiolitic basalts of which both the petrography and geochemistry made clear the environment of formation.

The fist data on the age of the sediments at the top of the basalts (Middle-Late Jurassic - Aptian-Cenomanian) of this area were presented 50 years ago (Boccaletti et al., 1966 and Bortolotti and Sagri, 1968), but no data on the petrology

and geochemistry of the volcanics were provided. Afterwards, only limited age data were obtained, using multidisciplinary approach (Rojay et al., 2001). As a consequence, ages from Middle Triassic to Cretaceous for the radiolarian cherts at the top of the basalts and very different environments for the genesis of the volcanics were found: mid-ocean ridge, seamount, supra-subduction zone, and back arc (e.g., Bragin and Tekin., 1996, Göncüoglu et al., 2001; 2008; 2010; Rojay et al., 2001; Tekin et al., 2002; Gökten and Floyd, 2007; Tekin and Göncüoglu, 2007; 2009; Yaliniz et al., 2000a).

## GEOLOGICAL BACKGROUND

The sampled ophiolitic outcrops of the Izmir-Ankara-Erzincan Suture Belt (IAESB) are located east of Ankara, (Fig. 1), where the concave shaped E-W trend of the belt between Izmir and Ankara makes a sudden loop and turns towards NNW, due to the Tertiary indentation (e.g., Cemen et al, 1993; Kaymakci et al., 2003) and anticlockwise rotation of the Kirşehir Massif.

The pre-Eocene evolution of this part of the IAESB was characterized by formation of a huge accretionary prism (for details see Rojay, 2013) between the northerly Sakarya Composite Terrane and the southerly Kütahya-Bolkardag Belt of the Anatolides, in the western part, and the Central Anatolian Crystalline Complex (CACC, Kirşehir Massif), in the eastern part. The initial juxtaposition of these oceanic and continental units is dated to the latest Cretaceous-Paleocene, however, compression and related thrusting lasted to the Miocene (Kocyigit et al., 1995).

The Sakaria Composite Terrane represents the active margin of the Izmir-Ankara Ocean, and was thrust over the IAESB both to the NNE of Ankara and to the SE of Çorum (Figs. 1, 2). It is a composite terrane comprising a Variscan arc complex and its Permian platform, as well as the Paleotethyan subduction-accretion prism (the Triassic Karakaya Complex, Göncüoglu et al., 2000; Okay and Göncüoglu, 2004). Its Jurassic to ?Late Cretaceous cover belonged to a north-facing passive continental margin that was transformed into an active margin by the northward subduction of the Izmir-Ankara oceanic lithosphere.

To the NNW of Ankara, the low-grade metamorphic greywackes of the Karakaya Complex are associated with Permian and Carboniferous limestone blocks and ocean island-type volcanic rocks with Carnian radiolarian cherts (e.g., Sayit et al., 2011). The unconformably overlying Mesozoic cover comprises from bottom to top: late Early Mid Jurassic neritic limestones, Late Jurassic - Early Cretaceous (e.g., Altiner et al., 1991) pelagic limestones and Late Cretaceous turbidites. The oldest common overstep sequence on the Izmir-Ankara-Erzincan Suture Belt (and the Sakarya Composite Terrane) is represented by Late Paleocene lagoonal sediments, which occur as discontinuous outcrops within the thrust zone between these two units (Göncüoglu et al., 2000).

In the northern-central part of the sampled area, the Sakarya Composite Terrane is represented by Late Jurassic - Early Cretaceous pelagic limestones (Sogukcam Limestone) that were thrust over the ophiolitic mélanges of the IAESB (Fig. 2). In this area, the Sakarya Composite Terrane is bounded by the branches of the right-lateral North Anatolian Transform Fault and occurs as E-W trending tectonic inlayers. East of the sampled area, to the SE of Çorum (Fig. 2), the metamorphic rocks of the Sakarya Composite Terrane (also known as Tokat Massif, Yilmaz et al., 1997) are tectonically overlying the ophiolitic mélange of the IAESB. In this area, Middle Eocene rocks are in turn unconformably overlying both units. However, the primary relations between the Sakarya and IAESB rocks are obscured by the intensive Oligocene strike-slip faulting.

The continental crust palinspastically located to the south and structurally lying below the IAESB units to the west of Ankara represents the northern edge of the Tauride-Anatolide Platform. It mainly consists of high pressure-low temperature metamorphosed tectonic slices (e.g., Okay and Tüysüz, 1999) with lithostratigraphic sequences resembling the Paleozoic-Mesozoic slope-type successions of the Ana-

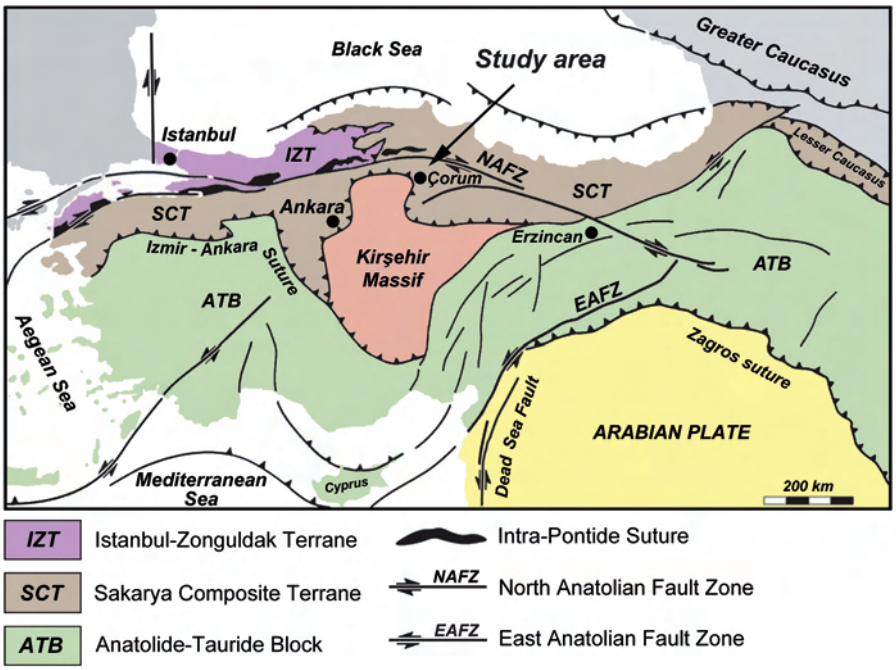


Fig. 1 - Main tectonic zones of Turkey (from Sengör and Yılmaz, 1981; Okay and Tüysüz, 1999; Göncüoğlu et al., 2012, modified).

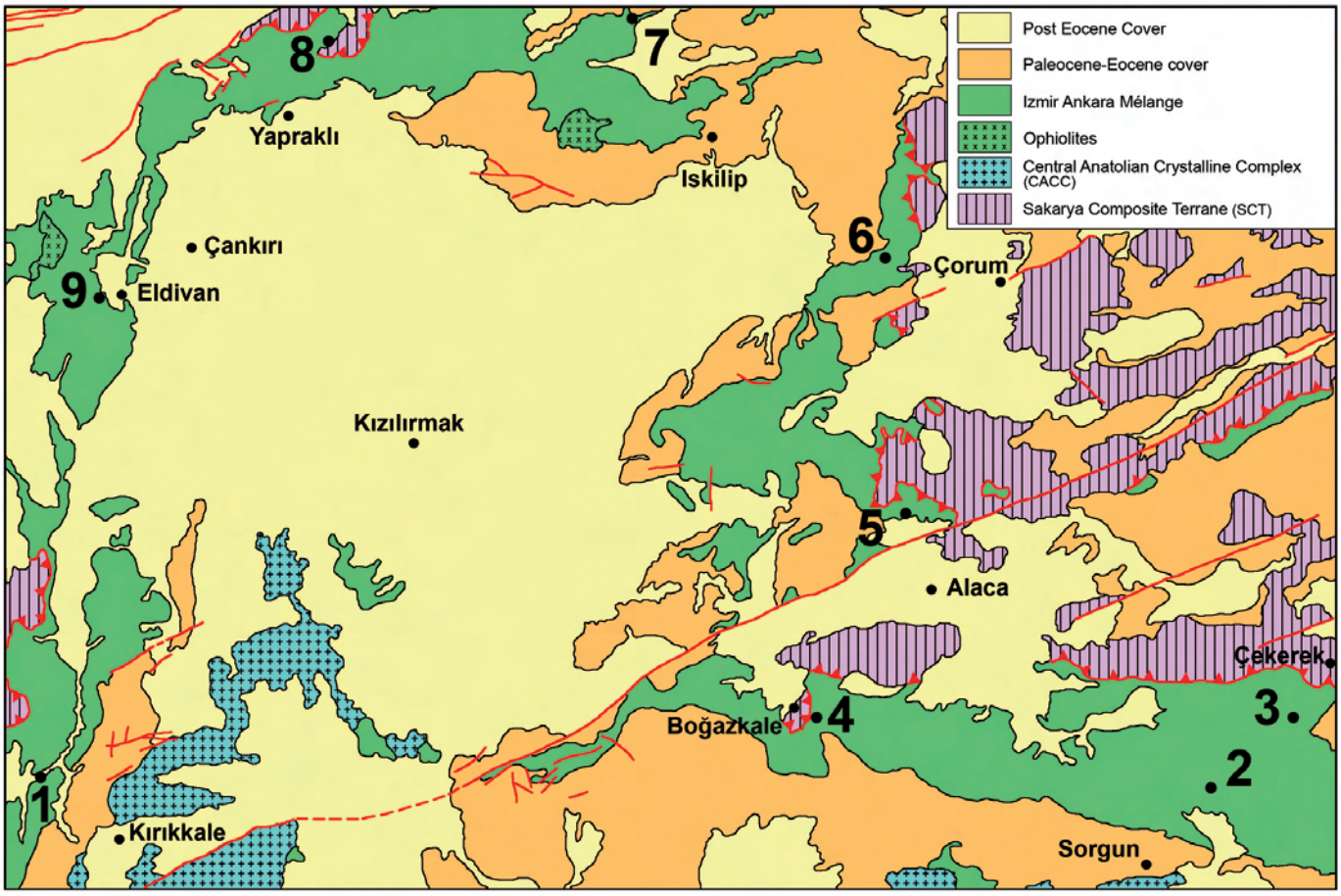


Fig. 2 - Sketch map of the study area (East of Ankara), with the main faults and thrusts and the location of the sampled sections (after 1/500.000 Geological Map of Turkey, MTA, modified).

tolides (Göncüoglu, 2011). In the sampled area (Fig. 2), the IAESB units are thrust onto the Central Anatolian Crystalline Complex (Yaliniz et al., 1996; 2000b), which is made of high temperature-medium pressure metamorphic successions resembling the Paleozoic-Mesozoic platform of the Tauride-Anatolide Platform. They were overthrust by Turonian supra-subduction type ophiolites, known as the Central Anatolian Ophiolites (Yaliniz et al., 2000a), which derived from the Izmir-Ankara Ocean. The basement rocks and the overlying ophiolite units were intruded by late Campanian granitoids (Köksal and Göncüoglu, 2008), indicating a Late Cretaceous initial obduction age. The oldest overstep sequences in this area are again post-Maastrichtian pre-Early Eocene (Gülyüz et al., 2012) red conglomerates, indicating a Paleocene age for the main juxtaposition of the CACC and IAESB mélange.

The IAESB rocks in the central part of the sampled area are covered by the Tertiary rocks of the Çankırı Basin, which include the Paleocene-Eocene post-orogenic marine clastic-volcanoclastics and carbonates, together with basaltic-andesitic volcanic rocks. On the other hand, the Neogene (Tortonian-Messinian) sediments cover the central part of the Çankırı Basin (e.g., Göncüoglu, 1992).

No geophysical data are available to interpret the thickness of the IAESB rocks that comprise the subducted and accreted remnants of the Izmir-Ankara oceanic lithosphere, together with island arc rocks and sedimentary rocks of a number of Late Cretaceous-Paleocene piggy-back basins (e.g., Cater et al., 1991; Erdogan et al., 1996).

## THE SAMPLED SECTIONS

The basaltic rocks and associated radiolarian cherts analysed in this paper come from the Izmir-Ankara Mélange. They were sampled from nine sections along the margins of the Çankırı Basin (Fig. 2) and described as follows.

***Section 1***

A metric intercalation of radiolarian cherts and siliceous shales in a massif of pillow basalts (with sheared contacts), road Elmadag - Kırıkkale (N 39°55.023 - E 33°21.989).

Samples: TU10.4, radiolarian chert; TU10.6, TU10.9, basalts.

***Section 2***

A metric intercalation of radiolarian cherts in a massif of pillow basalts, road Sorgun - Çekerek (Fig. 3b, N 39°54.889 - E 35°18.063).

Samples: TU10.12, radiolarian chert; TU10.14 - 17, basalts.

***Section 3***

Thin sequences basalts - radiolarian cherts in a block within the mélange, road Sorgun - Çekerek (near Gökdere) (N 39°59.924 - E 35°24.272) and (N 39°59.921 - E 35°24.274).

Samples: TU10.28, radiolarian chert; TU10.19, TU10.22 - 23 basalts.


Fig. 3 - a) Serpentinite mélange near Beynam; b) Pillow basalts along the road from Sorgun to Çekerek (Section 2); c) Overturned sequence of basalts and radiolarian cherts along the road from Çorum to Alaca (Section 5); d) Outcrop of basalts and radiolarian cherts along the road from Iskilip to Tosya (Section 7).

***Section 4***

Thin sequence basalts - radiolarian cherts with a sheared contact, 3 km from Boğazkale (N 40°00.377 - E 34°38.762).

Samples: TU10.31, chert; TU10.32 - 33, basalts.

***Section 5***

Overturned sequence radiolarian cherts - basalts in a big quarry, road Çorum to Alaca (south of Küre, Fig. 3c, N 40°15.861 - E 34°48.187).

Samples: TU10.36, chert; TU10.34, TU10.39 - 40, basalts.

***Section 6***

Small lens of cherts, without clear contacts, in a big mass of basalts, road Çorum - Iskilip (N 40°34.581 - E 34.46.574).

Samples: TU10.42, chert; TU10.44, basalt.

***Section 7***

Chert nodule in a basalt body, road Iskilip - Tosya (Fig. 3d, N 40°53.378 - E 34°20.756).

Samples: TU10.45, chert; TU10.46, basalt.

***Section 8***

Large outcrop of ophiolitic breccia with a siliceous matrix, northeast of Yapraklı (N 40°51.097- E 33°50.723).

Samples: TU10.47, chert; TU10.49a - 49b, basalt.

***Section 9***

Pillow basalts enveloped in reddish limestones, road Eldivan - Sabanozu (N 40°31.488 - E 33°28.106).

Samples: TU10.54 - 55, limestones; TU10.52 - 53, basalts.

## RADIOLARIAN BIOSTRATIGRAPHY

The radiolarian cherts were etched with hydrochloric and hydrofluoric acid at different concentrations following the method proposed by Dumitrica (1970), Pessagno and Newport (1972), Baumgartner et al. (1981), De Wever (1982). The samples yielded radiolarians with moderate preservation; the principal radiolarian markers are reported in Plate 1.

For taxonomy and ranges of the Late Triassic radiolarian markers we mainly refer to Carter (1993), Sugiyama (1997), Tekin (1999; 2002), Bragin (2007); for the taxonomy and ranges of the Late Jurassic-Early Cretaceous principal markers we refer to O'Dogherty (1994), Baumgartner et al. (1995a; 1995b), Dumitrica and Dumitrica-Jud (1995), Bak (1996; 1999), Dumitrica et al. (1997), Chiari et al. (2007), O'Dogherty et al. (2009a; 2009b), Robin et al. (2010), Bandini et al. (2011).

From the analyzed radiolarian cherts the following ages were obtained:

***Section 1***

*TU10.4*: late Valanginian to late Hauterivian (UAZ. 17-20; UAZones after Baumgartner et al., 1995b) for the presence of *Aurisaturnalis variabilis variabilis* (Squinabol) with *Hemicryptocapsa capita* Tan (Plate 1: 8 and 14).

***Section 2***

*TU10.12*: early-middle Bajocian to late Bathonian-early Callovian (UAZ. 3-7; UAZones after Baumgartner et al., 1995b) for the presence of *Stichomitra* (?) *takanoensis* Aita (Plate 1: 20).

***Section 3***

*TU10.28*: middle-late Oxfordian to late Kimmeridgian-early Tithonian (UAZ. 9-11; UAZones after Baumgartner et al., 1995b) for the occurrence of *Podocapsa amphitreptera* Foreman with *Fultacapsa sphaerica* (Ozvoldova) (Plate 1: 17 and 13).

***Section 4***

*TU10.31*: middle late Barremian-early early Aptian for the occurrence of *Aurisaturnalis carinatus perforatus* Dumitrica and Dumitrica Jud (range after Dumitrica and Dumitrica-Jud, 1995) (Plate 1: 7).

***Section 5***

*TU10.36*: early-early late Tithonian (UAZ. 12; UAZone after Baumgartner et al., 1995b) for the occurrence of *Cinguloturris cylindra* Kemkin and Rudenko, *Eucyrtidiellum pyramis* (Aita), *Ristola cretacea* (Baumgartner) with *Loopus primitivus* (Matsuoka and Yao) (Plate 1: 10, 12, 19 and 16).

***Section 6***

*TU10.42*: late Norian (*Betraccium deweveri* Zone; Zone after Carter, 1993) for the presence of *Betraccium deweveri* Pessagno and Blome and *Tetraporobrachia* sp. A sensu Carter (1993) (Plate 1: 2 and 5).

***Section 7***

*TU10.45*: Valanginian to middle Aptian-early Albian (Valanginian to *Costata* subzone of *Turbocapsula* Zone; Zone after O'Dogherty, 1994) for the presence of *Cryptamphorella clivosa* (Aliev) with *Praeconosphaera sphaeroconus* (Rüst) (Plate 1: 11 and 18).

***Section 8***

*TU10.47*: late Valanginian-early Barremian (UAZ. 17-21; UAZones after Baumgartner et al., 1995b) for the presence of *Cecrops septemporatus* (Parona) (Plate 1: 9).

## PETROGRAPHY, GEOCHEMISTRY AND TECTONO-MAGMATIC SIGNIFICANCE OF THE BASALTIC ROCKS

### Petrography

All the studied rocks were significantly affected by low-temperature, ocean-floor alteration, which resulted in the replacement of primary minerals, though primary igneous textures are well preserved. Plagioclase is usually replaced by either albite or calcite and rarely by clay mineral assemblages. Clinopyroxene is pseudomorphosed either by chlorite or actinolitic amphibole. However, in samples TU10.22 and TU10.23 (Section 3) clinopyroxene is replaced by brown hornblende, though fresh clinopyroxene relics are locally found. The groundmass secondary phases mainly consist of chlorite, and clay minerals. Regardless of the secondary mineralogical transformation, the following petrographic description of the various rock-types will be made on the bases of primary igneous phases. For a better understanding, it will be made according to the geochemical groups described in the Geochemistry section.

*Group 1*. Pillow and massive lavas have aphyric, microcrystalline sub-ophitic textures in which only small laths of plagioclase can be recognized. Pillow breccias are generally monogenetic and show coarse-grained, intergranular texture with euhedral plagioclase and interstitial clinopyroxene.

*Group 2*. Massive lavas show both aphyric and porphyritic (PI = ~ 40) textures. In both varieties, the groundmass texture is hyalopilitic. Phenocrysts are represented by large crystals of plagioclase. In all the studied rocks the crystallization order is: plagioclase + clinopyroxene ± Fe-Ti-oxides.

*Groups 3 and 4*. Pillow and massive lavas most commonly display aphyric, ophitic or sub-ophitic textures with crystal size ranging from microcrystalline to coarse-grained. Nonetheless, a few samples display slightly porphyritic textures with plagioclase microphenocrysts. In addition, hyalopilitic texture is locally observed. The groundmass mineral assemblage includes plagioclase, clinopyroxene, and variable amounts of opaque phases. Pillow breccias are generally monogenetic and the individual fragments are texturally and compositionally similar to the pillow lavas. These rocks are characterized by variable abundance of varioles filled by calcite.

### Analytical methods

Whole-rock major and some trace element analyses were obtained by X-ray fluorescence (XRF) on pressed-powder pellets, using an ARL Advant-XP automated X-ray spectrometer. The matrix correction methods proposed by Lachance and Trail (1966) were applied. Volatile contents were determined as loss on ignition (L.O.I.) at 1000°C.

The $CO_2$ content was determined by simple volumetric technique (Jackson, 1958) only on samples affected by calcite veins and amygdales. This technique was calibrated using standard amounts of reagent grade $CaCO_3$. In addition, for the discussion of the geochemical characteristics and for a better comparison of chemical data, the major element composition of these samples were recalculated on calcite-free basis. In detail, CaO content in secondary calcite has been calculated according to stoikiometric proportions with $CO_2$ contents, given that the secondary carbonates consist exclusively of calcite. Major element composition has then been re-calculated to 100 wt% without considering L.O.I. and CaO in calcite.

Accuracy of the data and detection limits for XRF and $CO_2$ analyses were evaluated using results for international standard rocks, duplicate runs of several samples, and the blind standards included in the sample set; results are given in Table 1. Whole-rock analyses were performed at the Phisics and Earth Science Dept. of the University of Ferrara (Dipartimento di Fisica e Scienze della Terra, Università di Ferrara). The results are shown in Table 1.

### Geochemistry

The following geochemical description is made mainly using those elements that are virtually immobile during

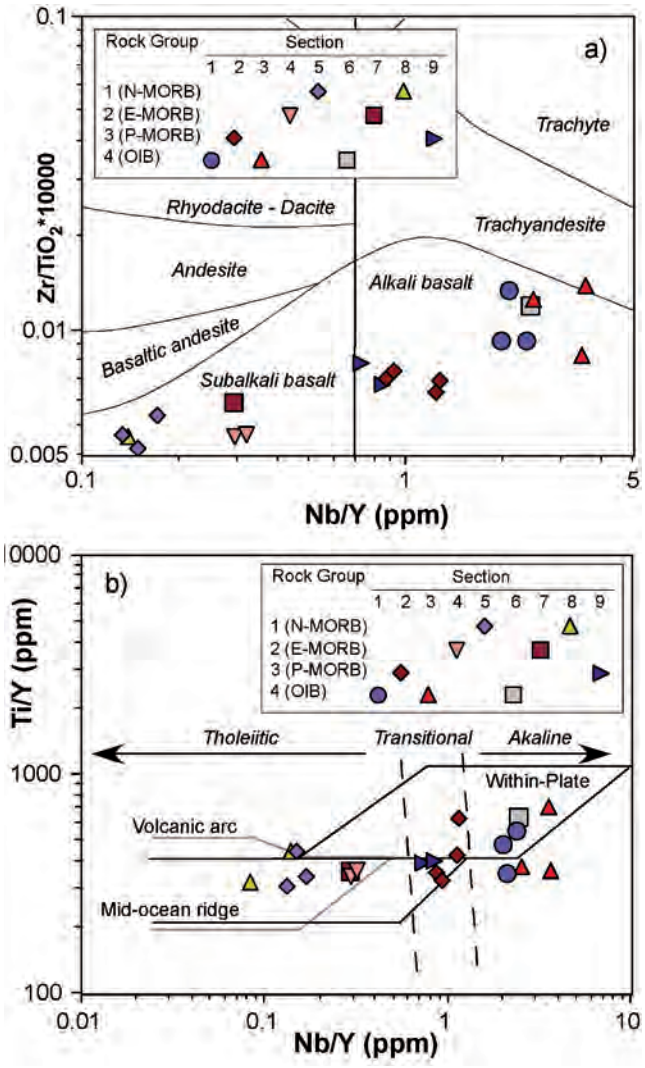


Fig. 4 - a) $Zr/TiO_2*10000$ vs. Nb/Y (after Winchester and Floyd, 1977) and b) Ti/Y vs. Nb/Y (after Pearce, 1982) discrimination diagrams for volcanic and subvolcanic rocks from the Izmir-Ankara Mélange.

low-temperature alteration and metamorphism (e.g., Pearce and Norry, 1979). These elements include many incompatible elements, such as: Ti, P, Zr, Y, Sc, Nb, Hf, Th, as well as some transition metals (e.g., Ni, Co, Cr, V).

Due to the mobilization of most major elements during alteration and metamorphism, the standard classification based on $SiO_2$ cannot be used. Therefore, the studied rocks are classified using diagrams based on immobile incompatible elements (Fig. 4a). Using these discrimination diagrams, four groups of volcanic rocks can be recognized, as follows.

*Group 1* is represented by subalkaline basalts (Fig. 4a) cropping out in sections 5 and 8. The sub-alkaline nature of these rocks is clearly testified by very low Nb/Y ratios (Fig. 4a, b). They have rather evolved compositions, characterized by relatively high contents of incompatible elements such as $TiO_2$, $P_2O_5$, and Y, as well as $FeO_t$, (Table 1, Fig. 5). The low Mg# also indicate that these basalts do not correspond to primary magmas in equilibrium with mantle compositions (Mg# = 0.68-0.75). With respect to their $TiO_2$ and $P_2O_5$ contents, these basalts display a tholeiitic character. A limited evolutionary trend can be observed in the variation diagrams of Fig. 5. These trends are characterized by significant variation of $FeO_t$, Y, Ni contents and Mg# with limited Zr (here assumed as representative of fractionation) and $TiO_2$ contents. Ni and Cr contents are relatively high in samples from Section 5, whereas they are low in samples from Section 8, though all samples have comparable Mg#. V content is generally high (Table 1). In contrast, Nb, La, and Ce contents are generally low. Group 1 basalts are characterized by N-MORB (normal mid-ocean ridge basalt) normalized incompatible element patterns, which are rather flat from Nb to Y (Fig. 6a). The overall geochemical features of these rocks, as well as their incompatible element patterns resemble those of typical N-MORB (Sun and McDonough, 1989).

*Group 2* is represented by the subalkaline basalts (Fig. 4a) cropping out in Sections 4 and 7. These rocks have a sub-alkaline nature with low Nb/Y ratios (Fig. 4b) and show relatively high $TiO_2$, $P_2O_5$, and Y contents (Table 1, Fig. 5). Ni, though variable, is generally low, whereas Cr and V are rather high. Basalts from Section 4 have low Mg# indicating that they most likely represent rather evolved magmas. In contrast, the basalt from Section 7 shows rather high Mg# and coherently it shows lower $TiO_2$, $FeO_t$, Y, and V compared to basalts from Section 4. Most element concentrations and the evolutionary trend (Fig. 5) of Group 2 rocks are similar to those of Group 1 basalts. However, as a distinctive feature, Group 2 basalts display N-MORB-normalized incompatible element contents (Fig. 6b), similar to those of E-MORBs (enriched-type MORBs). Indeed, they show patterns smoothly decreasing from Ba to Y.

*Group 3* is represented by alkaline basalts and ferrobasalts from Section 2, as well as alkaline basalts from Section 9 (Fig. 4a). These rocks have a transitional nature, as testified by their high Nb/Y ratios (Fig. 4b). Alkaline basalts from Section 2 display rather primitive compositions with relatively high Mg# and high $TiO_2$, $P_2O_5$, Zr, Nb, Hf, and Th contents (Table 1, Fig. 5). In contrast, ferrobasalts from Section 2 and alkaline basalts from Section 9 have rather evolved compositions, with relatively low Mg# and very high $TiO_2$, $P_2O_5$, Zr, Nb, Hf, and Th contents (Table 1, Fig. 5). Accordingly, Ni and Cr contents are generally high in basalts, whereas they are relatively low in the differentiated rocks. Except for Mg#, the variations of many elements with respect to Zr display common evolutionary trends towards high contents of the incompatible elements and $FeO_t$ and low contents of the compatible elements for all Group 3 samples (Fig. 5). These trends are compatible with a magmatic evolution by fractional crystallization. Group 3 rocks show high abundance in LFSE with respect to N-MORB and display regularly decreasing N-MORB normalized patterns from Rb to Y (Fig. 6c). The less enriched samples show patterns comparable with those of P-MORB (plume-type MORB) and the most enriched samples have incompatible element contents similar to those of alkaline basalts generated at within-plate ocean island settings (OIB).

*Group 4* is represented mainly by alkaline basalts and subordinate trachyandesites from Sections 1, 3, and 6 (Fig. 4a). These rocks have a clear alkaline nature, as testified by their very high Nb/Y ratios (Fig. 4b). Alkaline basalts from Sections 3 and 6 mainly display relatively primitive compositions, whereas alkaline basalts from Section 1 represent rather evolved compositions. All samples have generally high contents of $TiO_2$, $P_2O_5$, Zr, Nb, Hf, Th and low contents of compatible elements (Table 1, Fig. 5).

In the variation diagrams, rocks from the different sections show different evolutionary trends, most likely reflecting the distinct evolution of magmas of different initial compositions. This is particularly evident in the $TiO_2$, Y,

Table 1 - Representative major and trace element analyses of volcanic rocks from the Izmir-Ankara Mélange.

| Section | 1 | | | 2 | | | | 3 | | | 4 | |
|---|---|---|---|---|---|---|---|---|---|---|---|---|
| Sample | TU10-6 | TU10-9 | TU10-10 | TU10-14 | TU10-15 | TU10-16 | TU10-17 | TU10-19 | TU10-22 | TU10-23 | TU10-32 | TU10-33 |
| Rock | bas | tra | bas | bas | bas | Fe-bas | Fe-bas | tra and | bas | bas | bas | bas |
| Group | 4 | 4 | 4 | 3 | 3 | 3 | 3 | 4 | 4 | 4 | 2 | 2 |
| Type | alk | alk | alk | trans | trans | trans | trans | alk | alk | alk | subalk | subalk |
| | OIB | OIB | OIB | P-MORB | P-MORB | P-MORB | P-MORB | OIB | OIB | OIB | E-MORB | E-MORB |
| Age | E Cr | | | M-L Jr | M-L Jr | M-L Jr | M-L Jr | | L Jr | | E Cr | E Cr |
| Note | pillow | breccia | pillow | pillow | pillow | pillow | pillow | MLF | pillow | pillow | MLF | MLF |
| $SiO_2$ | 41.40 | 56.12 | 39.61 | 44.12 | 40.20 | 42.40 | 44.87 | 44.36 | 46.03 | 44.81 | 45.98 | 46.18 |
| $TiO_2$ | 1.91 | 2.35 | 1.96 | 2.28 | 1.65 | 3.27 | 2.55 | 2.97 | 2.32 | 2.21 | 1.51 | 1.46 |
| $Al_2O_3$ | 11.76 | 15.96 | 11.81 | 14.48 | 11.92 | 13.81 | 13.82 | 13.41 | 17.06 | 16.49 | 13.44 | 13.30 |
| $Fe_2O_3$ | 0.93 | 1.33 | 1.00 | 1.74 | 1.00 | 2.08 | 1.96 | 1.45 | 1.42 | 1.40 | 1.44 | 1.26 |
| FeO | 6.18 | 8.90 | 6.67 | 11.60 | 6.66 | 13.89 | 13.06 | 9.63 | 9.47 | 9.31 | 9.61 | 8.43 |
| MnO | 0.15 | 0.11 | 0.12 | 0.23 | 0.22 | 0.19 | 0.19 | 0.40 | 0.20 | 0.20 | 0.29 | 0.27 |
| MgO | 4.24 | 1.68 | 3.86 | 9.25 | 6.32 | 7.42 | 9.98 | 9.14 | 7.31 | 9.05 | 5.69 | 5.14 |
| CaO | 16.69 | 3.61 | 17.84 | 8.16 | 18.02 | 8.04 | 6.23 | 6.96 | 6.48 | 7.45 | 14.15 | 15.60 |
| $Na_2O$ | 3.73 | 7.37 | 2.93 | 2.39 | 2.11 | 3.07 | 1.74 | 3.24 | 2.07 | 1.84 | 2.82 | 3.21 |
| $K_2O$ | 1.72 | 0.65 | 2.06 | 0.82 | 1.89 | 0.69 | 1.26 | 1.13 | 3.54 | 2.95 | 0.46 | 0.40 |
| $P_2O_5$ | 0.48 | 0.59 | 0.60 | 0.33 | 0.21 | 0.54 | 0.62 | 0.52 | 0.96 | 0.86 | 0.14 | 0.13 |
| L.O.I. | 10.94 | 1.16 | 11.56 | 4.65 | 9.89 | 4.65 | 3.73 | 6.94 | 3.15 | 3.50 | 4.58 | 4.66 |
| Total | 100.13 | 99.84 | 100.03 | 100.05 | 100.08 | 100.05 | 100.01 | 100.15 | 100.01 | 100.06 | 100.11 | 100.06 |
| $CO_2$ | 6.23 | – | 6.13 | – | 7.05 | – | – | – | – | – | 1.80 | 2.27 |
| Mg# | 55.0 | 25.2 | 50.8 | 58.7 | 62.9 | 48.8 | 57.7 | 62.8 | 57.9 | 63.4 | 51.4 | 52.1 |
| Zn | 73 | 104 | 57 | 72 | 63 | 110 | 101 | 109 | 75 | 72 | 84 | 87 |
| Cu | 25 | 35 | 44 | 77 | 71 | 59 | 57 | 69 | 40 | 40 | 77 | 94 |
| Sc | 23 | 9 | 18 | 36 | 40 | 43 | 35 | 36 | 8 | 10 | 42 | 39 |
| Ga | 15 | 14 | 16 | 21 | 15 | 24 | 20 | 16 | 17 | 19 | 16 | 14 |
| Ni | 70 | 26 | 54 | 78 | 53 | 8 | 11 | 100 | 25 | 42 | 139 | 139 |
| Co | 27 | 16 | 23 | 37 | 33 | 37 | 30 | 36 | 23 | 25 | 39 | 41 |
| Cr | 227 | 56 | 115 | 135 | 81 | 26 | 21 | 271 | 16 | 29 | 389 | 371 |
| V | 204 | 180 | 206 | 334 | 275 | 403 | 329 | 382 | 188 | 210 | 390 | 377 |
| Rb | 29 | 12 | 33 | 9 | 15 | 8 | 16 | 29 | 75 | 60 | 5 | 5 |
| Ba | 289 | 186 | 340 | 246 | 717 | 199 | 177 | 193 | 1975 | 1379 | 83 | 75 |
| Th | 6 | 9 | 5 | 3 | 4 | 7 | 5 | 9 | 9 | 10 | n.d. | n.d. |
| Nb | 57 | 83 | 62 | 32 | 39 | 50 | 45 | 95 | 142 | 91 | 9 | 9 |
| La | 38 | 64 | 31 | 23 | 21 | 35 | 38 | 47 | 65 | 56 | 7 | 5 |
| Ce | 73 | 192 | 76 | 45 | 43 | 82 | 76 | 89 | 160 | 118 | 16 | 12 |
| Pb | 4 | 7 | 5 | 7 | 4 | 7 | 6 | 16 | 8 | 7 | 4 | 3 |
| Sr | 600 | 441 | 494 | 302 | 292 | 391 | 371 | 216 | 740 | 749 | 131 | 136 |
| Nd | 27 | 45 | 27 | 19 | 16 | 33 | 30 | 32 | 60 | 49 | 9 | 9 |
| Zr | 217 | 320 | 225 | 165 | 128 | 239 | 196 | 265 | 330 | 287 | 74 | 73 |
| Y | 29 | 40 | 26 | 28 | 33 | 58 | 48 | 27 | 39 | 36 | 29 | 27 |
| Hf | 4 | 10 | 4 | 6 | 3 | 8 | 7 | 6 | 8 | 6 | 3 | 3 |

bas- basalt; Fe-bas- ferrobasalt; tra and- trachyandesite; tra bas- trachybasalt; al-; alkaline-type; trans- transitional-type; subalk- subalkaline-type; OIB- ocean island basalt; P-MORB- plume-type mid-ocean ridge basalt; E-MORB- enriched-type mid-ocean ridge basalt; N-MORB- normal-type mid-ocean ridge basalt; E- Early; M- Middle; L- Late; Jr- Jurassic; Cr- Cretaceous; MLF- massive lava flow; n.d.- not detected; - not analyzed. Mg# = $100xMg/(Mg+Fe^{2+})$. $Fe_2O_3 = 0.15xFeO$. Detection limits (major oxides = wt%; trace elements = ppm) and accuracy (mean absolute relative %), evaluated using results for international standard rocks, duplicate runs of several samples, and the blind standards included in the sample set are also reported.

and Ni vs. Zr diagrams where different Zr vs. element ratios further support this conclusion. Nonetheless, the well-defined trends observed for samples from each single section suggest that each section consists of rocks belonging to a comagmatic suite. Group 4 rocks show high abundance in LFSE with respect to N-MORB and display regularly decreasing N-MORB normalized patterns from Rb to Y (Fig. 6d). Compared with Group 3 rocks, these basalts show slightly higher LILE (large ion lithophile elements) concentrations. N-MORB normalized patterns are comparable with those of alkaline basalts generated at within-plate ocean island settings (OIB).

## Tectono-magmatic interpretation

One of the main goals of this study is to assess the nature and tectonic significance of the magmatic events that occurred in the Turkish sector of the Tethys. According to many authors (e.g., Pearce, 1982), the compositional differences between magma types depend on different source characteristics that are associated, in turn, to distinct tectono-magmatic settings of formation. We will therefore focus our discussion on the tectonic setting of formation of the four distinct lava groups identified in the previous chapter.

Table 1 *(continued)*

| Section | 5 | | | 6 | 7 | 8 | | 9 | | | |
|---|---|---|---|---|---|---|---|---|---|---|---|
| Sample | TU10-34 | TU10-39 | TU10-40 | TU10-44 | TU10-46 | TU10-49a | TU10-49b | TU10-52 | TU10-53 | detection | accuracy |
| Rock | bas | bas | bas | tra bas | bas | bas | bas | bas | bas | limit | (relative %) |
| Group | 1 | 1 | 1 | 4 | 2 | 1 | 1 | 3 | 3 | | |
| Type | subalk N-MORB | subalk N-MORB | subalk N-MORB | alk OIB | subalk E-MORB | subalk N-MORB | subalk N-MORB | trans P-MORB | trans P-MORB | | |
| Age | L Jr-E Cr | L Jr-E Cr | L Jr-E Cr | Norian | E Cr | E Cr | E Cr | | | | |
| Note | MLF | breccia | MLF | MLF | MLF | pillow | pillow | MLF | MLF | | |
| $SiO_2$ | 47.04 | 48.28 | 46.35 | 54.95 | 48.35 | 53.76 | 48.67 | 48.72 | 39.89 | 0.05 | 3 |
| $TiO_2$ | 1.48 | 1.46 | 1.74 | 2.06 | 1.20 | 1.51 | 1.46 | 1.89 | 1.37 | 0.01 | 3 |
| $Al_2O_3$ | 13.50 | 14.84 | 15.70 | 16.47 | 17.65 | 13.26 | 13.83 | 17.70 | 11.71 | 0.05 | 7 |
| $Fe_2O_3$ | 1.28 | 1.42 | 1.59 | 0.51 | 0.77 | 1.28 | 1.65 | 1.42 | 1.05 | 0.10 | 3 |
| FeO | 8.51 | 9.49 | 10.60 | 3.40 | 5.14 | 8.52 | 11.01 | 9.49 | 6.97 | | |
| MnO | 0.26 | 0.19 | 0.11 | 0.20 | 0.11 | 0.13 | 0.16 | 0.05 | 0.17 | 0.05 | 7 |
| MgO | 5.24 | 5.48 | 2.40 | 3.05 | 4.69 | 5.80 | 7.48 | 3.77 | 4.26 | 0.01 | 7 |
| CaO | 15.85 | 9.28 | 12.16 | 5.74 | 9.55 | 8.03 | 6.18 | 4.16 | 21.76 | 0.04 | 3 |
| $Na_2O$ | 3.27 | 3.39 | 3.77 | 4.99 | 5.71 | 3.88 | 2.49 | 2.04 | 1.88 | 0.01 | 7 |
| $K_2O$ | 0.41 | 1.49 | 1.31 | 4.50 | 0.29 | 0.36 | 0.88 | 4.64 | 0.53 | 0.01 | 3 |
| $P_2O_5$ | 0.14 | 0.17 | 0.28 | 0.34 | 0.12 | 0.17 | 0.11 | 0.32 | 0.14 | 0.01 | 7 |
| L.O.I. | 3.02 | 4.56 | 3.94 | 3.81 | 6.45 | 3.20 | 6.02 | 5.83 | 10.28 | 0.5 | 4 |
| Total | 100.00 | 100.05 | 99.95 | 100.00 | 100.03 | 99.89 | 99.94 | 100.04 | 100.01 | | |
| $CO_2$ | 0.95 | – | 0.93 | – | – | – | – | – | 7.00 | 0.24 | 2 |
| Mg# | 52.3 | 50.7 | 28.8 | 61.5 | 61.9 | 54.8 | 54.8 | 41.4 | 52.2 | | |
| Zn | 87 | 115 | 124 | 54 | 63 | 79 | 97 | 115 | 63 | 2 | 6 |
| Cu | 92 | 62 | 27 | 22 | 95 | 55 | 12 | 35 | 27 | 3 | 6 |
| Sc | 44 | 55 | 48 | 3 | 26 | 19 | 40 | 28 | 32 | 3 | 6 |
| Ga | 16 | 18 | 17 | 17 | 14 | 21 | 18 | 16 | 19 | 4 | 6 |
| Ni | 139 | 106 | 69 | 3 | 40 | 32 | 15 | 140 | 213 | 2 | 4 |
| Co | 41 | 33 | 32 | 8 | 33 | 26 | 24 | 35 | 36 | 2 | 6 |
| Cr | 372 | 197 | 273 | 10 | 266 | 67 | 18 | 392 | 305 | 1 | 4 |
| V | 370 | 300 | 368 | 147 | 194 | 232 | 380 | 317 | 333 | 2 | 4 |
| Rb | 26 | 30 | 17 | 80 | 2 | 2 | 16 | 71 | 2 | 1 | 5 |
| Ba | 73 | 69 | 130 | 1184 | 132 | 116 | 173 | 274 | 85 | 3 | 12 |
| Th | n.d. | n.d. | 1 | 7 | n.d. | n.d. | n.d. | 3 | 3 | 1 | 8 |
| Nb | 4 | 5 | 5 | 48 | 6 | 4 | 3 | 25 | 19 | 1 | 10 |
| La | 3 | 4 | 3 | 39 | 5 | 3 | 3 | 18 | 13 | 3 | 12 |
| Ce | 8 | 10 | n.d. | 79 | 13 | 9 | 9 | 28 | 31 | 5 | 12 |
| Pb | 3 | 5 | 2 | 30 | 3 | 5 | 6 | 6 | 6 | 3 | 14 |
| Sr | 136 | 393 | 201 | 592 | 543 | 120 | 132 | 164 | 96 | 2 | 5 |
| Nd | 9 | 10 | 13 | 25 | 8 | 10 | 11 | 19 | 10 | 5 | 10 |
| Zr | 65 | 82 | 85 | 258 | 75 | 71 | 80 | 135 | 132 | 2 | 5 |
| Y | 27 | 31 | 40 | 20 | 21 | 29 | 36 | 30 | 26 | 1 | 3 |
| Hf | n.d. | 3 | n.d. | 5 | 4 | 3 | n.d. | 5 | n.d. | 3 | 11 |

Some discrimination diagrams are illustrated in Fig. 7. When used independently, these diagrams show slightly different results. However, when combined they provide a powerful tool for interpreting the tectonic setting of formation of the studied rocks. Group 1 and Group 2 rocks plot in the fields for N-MORB and E-MORB, respectively in both Fig. 7a (Meschede, 1986) and Fig. 7b (Cabanis and Lécolle, 1989), whereas in Fig. 7c (Shervais, 1982) they collectively plot in the field for MORB. Group 4 rocks form a clearly defined set of within-plate alkaline basalts in all diagrams. Group 3 basalts plot in the fields for OIB in Fig. 7a, b, whereas they plot in the field for MORB in Fig. 7c. Nonetheless, in all these diagrams, this rock group forms a consistent field, which is separate from the other rocks groups. Fig. 7b has the highest potential in defining rocks ranging from N-MORB to OIB compositions.

The six samples of Group 3, despite their high Nb contents similar to those of alkaline OIBs, have Ti and V contents similar to those of MORBs. These geochemical features, coupled with the general geochemistry of these rocks, which is transitional between E-MORBs and OIBs suggest a P-MORB affinity for Group 3. In summary, the four different groups of volcanic rocks from the Izmir-Ankara Mélange show different geochemical affinities; precisely: N-MORB (Group 1); E-MORB (Group 2), P-MORB (Group 3), and OIB (Group 4).

Some highly incompatible element ratios (e.g., Zr/Nb, Ce/Y, Zr/Y, Nb/Y) are little affected by fractional crystallization of predominantly olivine + clinopyroxene + plagioclase. Therefore, even with significant amounts of fractionation, they are believed to represent the elemental ratios in the source (e.g., Allègre and Minster, 1978). The different rock groups can therefore be characterized using ratios of highly incompatible elements, such as Ce/Y and Nb/Y (Fig. 8).

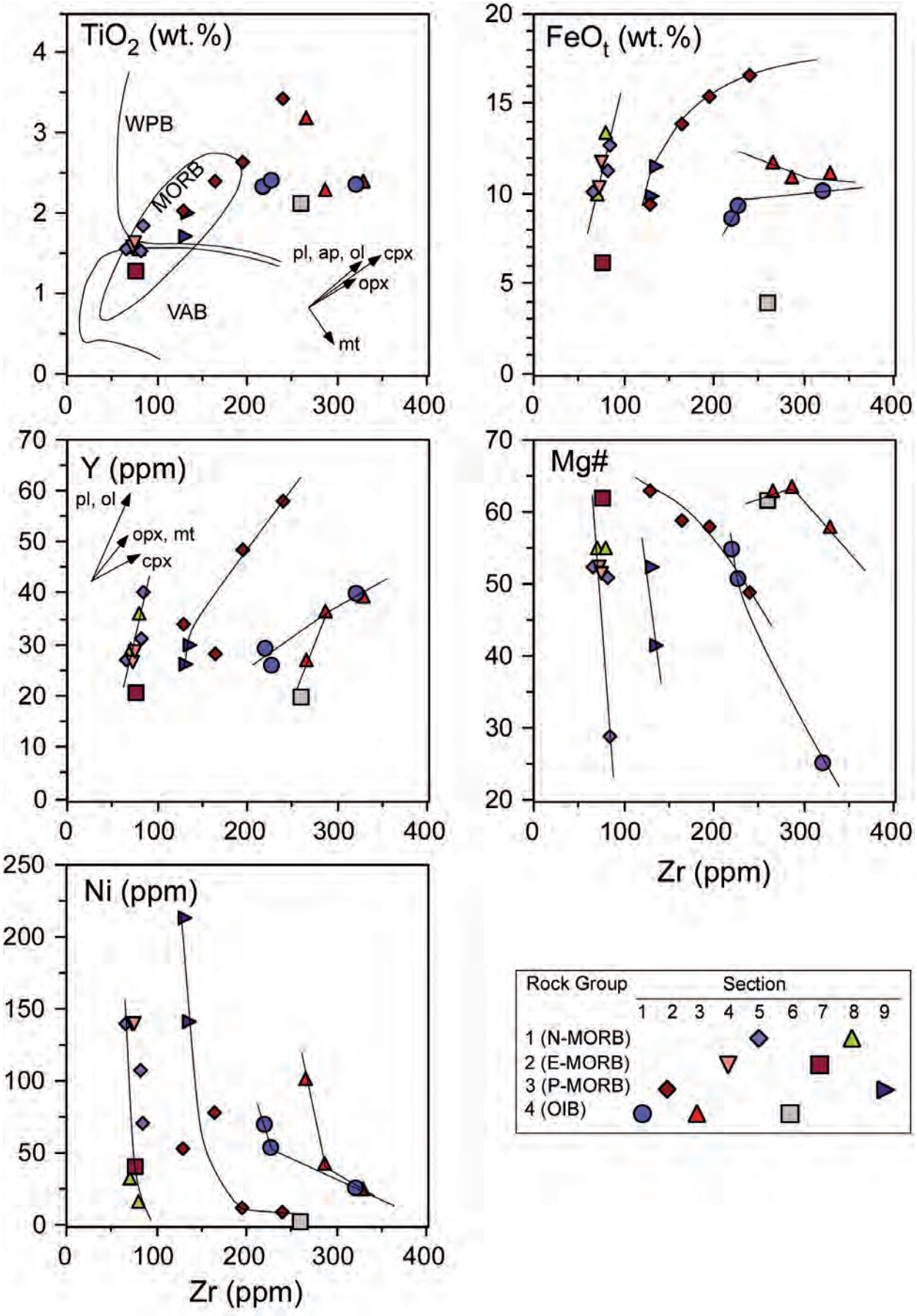


Fig. 5 - Variation diagrams for some representative major and trace elements. MORB (mid-ocean ridge basalts), VAB (volcanic arc basalts) and WPB (within plate basalts) compositional fields and fractionation vectors are from Pearce (1982). pl- plagioclase; ol- olivine; ap- apatite; cpx- clinopyroxene; opx- orthopyroxene; mt- magnetite. Mg# = 100xMg/(Mg + $Fe^{2+}$). Inferred fractionation trends for the different rock-groups are also shown.

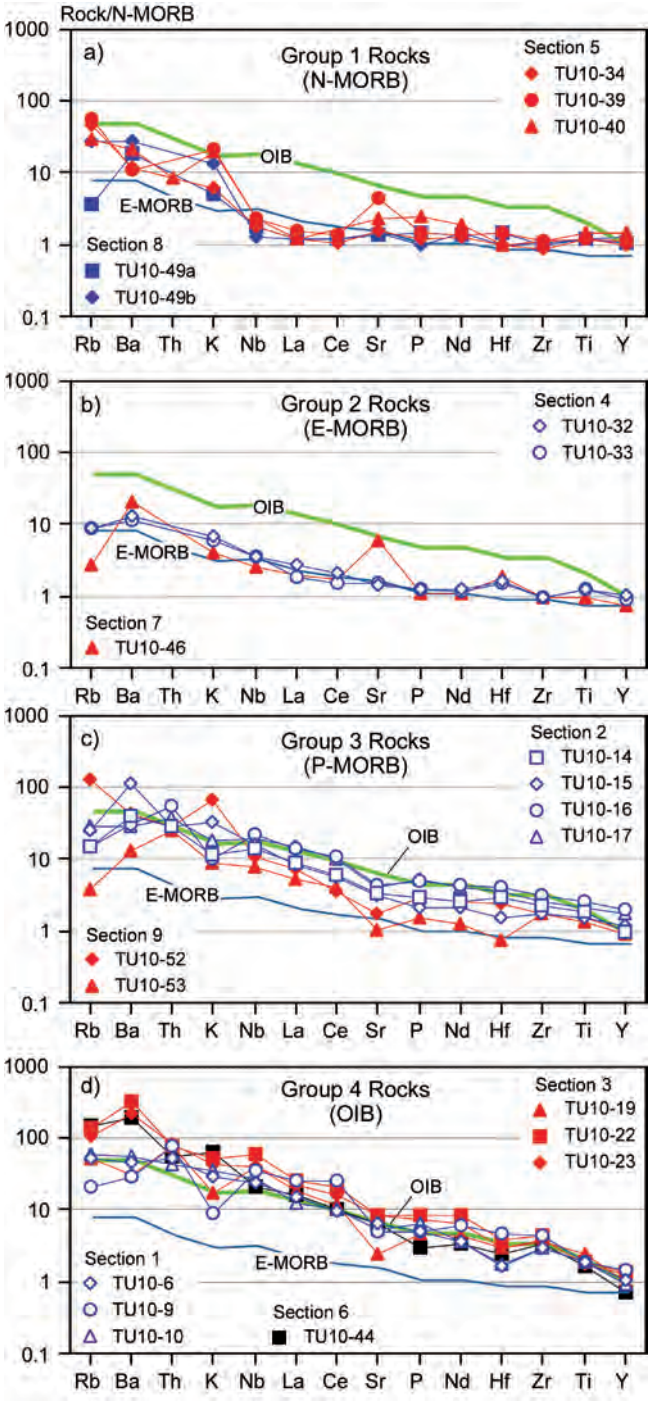


Fig. 6 - N-MORB normalized incompatible element patterns for volcanic rocks from the Izmir-Ankara Mélange. Normalizing values and compositions of enriched mid-ocean ridge basalt (E-MORB), and ocean-island basalt (OIB) are from Sun and McDonough (1989).

In this figure is apparent how the different rock groups form distinct clusters. Both Ce/Y and Nb/Y ratios increase from N-MORBs to E-MORBs, P-MORBs, and OIBs. These ratios, as well as the distinct normalized multi-element and REE patterns (Fig. 6) suggest that the different Groups of volcanic rocks from the Izmir-Ankara Mélange most likely originated from chemically distinct mantle sources. In N-MORBs, Ce/Y and Nb/Y ratios are low and consistent with a depleted mantle source, whereas, increasing elemental ratios in the other rock groups reflect progressive enrichment of the mantle source from E-MORBs to P-MORBs and OIBs.

The co-variation of Zr/Y vs. Zr in Izmir-Ankara Mélange basalts (Fig. 9) is then used for evaluating the depleted vs. enriched nature of the possible mantle sources of the different rock groups. N-MORBs are compatible with compositions of melts generated by partial melting of a depleted MORB mantle source (DMM, Workman and Hart, 2005). In contrast, OIBs are compatible with partial melting of enriched-type mantle sources (EM). E-MORBs may have derived from a mantle source slightly enriched with respect to a DMM source, whereas P-MORBs are compatible with melts generated from a mantle source significantly enriched, compared to DMM. Similar associations of N-, E-, P-MORBs and OIBs are widespread in the eastern Neo-Tethys ophiolites, as they are found in many ophiolitic complexes from the Albanides-Hellenides (Photiades et al., 2003; Bortolotti et al., 2004; 2006; 2008; Saccani and Photiades, 2005; Saccani et al., 2008; Tashko et al., 2009; Chiari et al., 2012), Turkey (Tankut et al., 1998; Yaliniz et al., 2000a; Rojay et al., 2001; Gökten and Floyd, 2007; Aldanmaz et al., 2008; Dangerfield et al., 2011), Iran (Arvin and Robinson, 1994; Allahyari et al., 2010; Saccani et al., 2010; 2013a) and Oman (Lapierre et al., 2004; Chauvet et al., 2011). Moreover, similar rock associations also characterize the Paleo-Tethys ophiolites in Iran (Saccani et al., 2013b). These associations of depleted and variably enriched rocks represent volcanic products erupted either in oceanic settings or in continental rift settings. They are interpreted as the result of partial melting of a MORB-type asthenospheric source, locally enriched in HFSE (high field strength element) and LREE (light rare earth elements) by an OIB-type component (plume-type component). The co-variation of Zr/Y and Zr/Nb in the Izmir-Ankara Mélange basalts (Fig. 10) is then used to qualitatively depict the influence of a plume-type component on MORB compositions. From Fig. 10 it is evident that the data conform extremely well to the mixing curve calculated using the OIB and N-MORB end-members. Such mixing relationships are consistent with either magma mixing or source region mixing. The composition of Group 4 alkaline rocks is consistent with a genesis from an OIB-type mantle source.

In contrast, sample TU10.49b of Group 1 N-MORB from Section 8 has elemental ratios consistent with a genesis from a pure DMM source. The slight shifting of Group 1 sample TU10.49a from Section 8 towards comparatively more enriched compositions (Fig. 10) is likely due to the slightly fractionated composition of this sample ($SiO_2$ = 53.76 wt%). Other N-MORBs from Section 5 overlap the compositional field for E-MORB, therefore it cannot be excluded that these rocks may have been affected by a little OIB-type compositional influence. However, the incompatible element general composition (Fig. 6a) indicates that such an eventual OIB-type influence was negligible. In contrast, E- and P-MORBs have elemental ratios reflecting variable interactions between DMM- and OIB-type sources.

## AGE CONSTRAINTS

The ages obtained for the studied radiolarian assemblages are mainly Early Cretaceous, with one finding of Late Triassic and three of Middle-Late Jurassic. These ages are in agreement with the radiolarians (Bragin and Tekin, 1996; Tekin, 1999; Celik, 2010; Uner, 2010; Tekin et al., 2012) and foraminifera (Boccaletti et al., 1966; Bortolotti and Sagri, 1968; Yaliniz et al., 2000b; Rojay et al., 2001) data obtained from different parts of the IAESB.

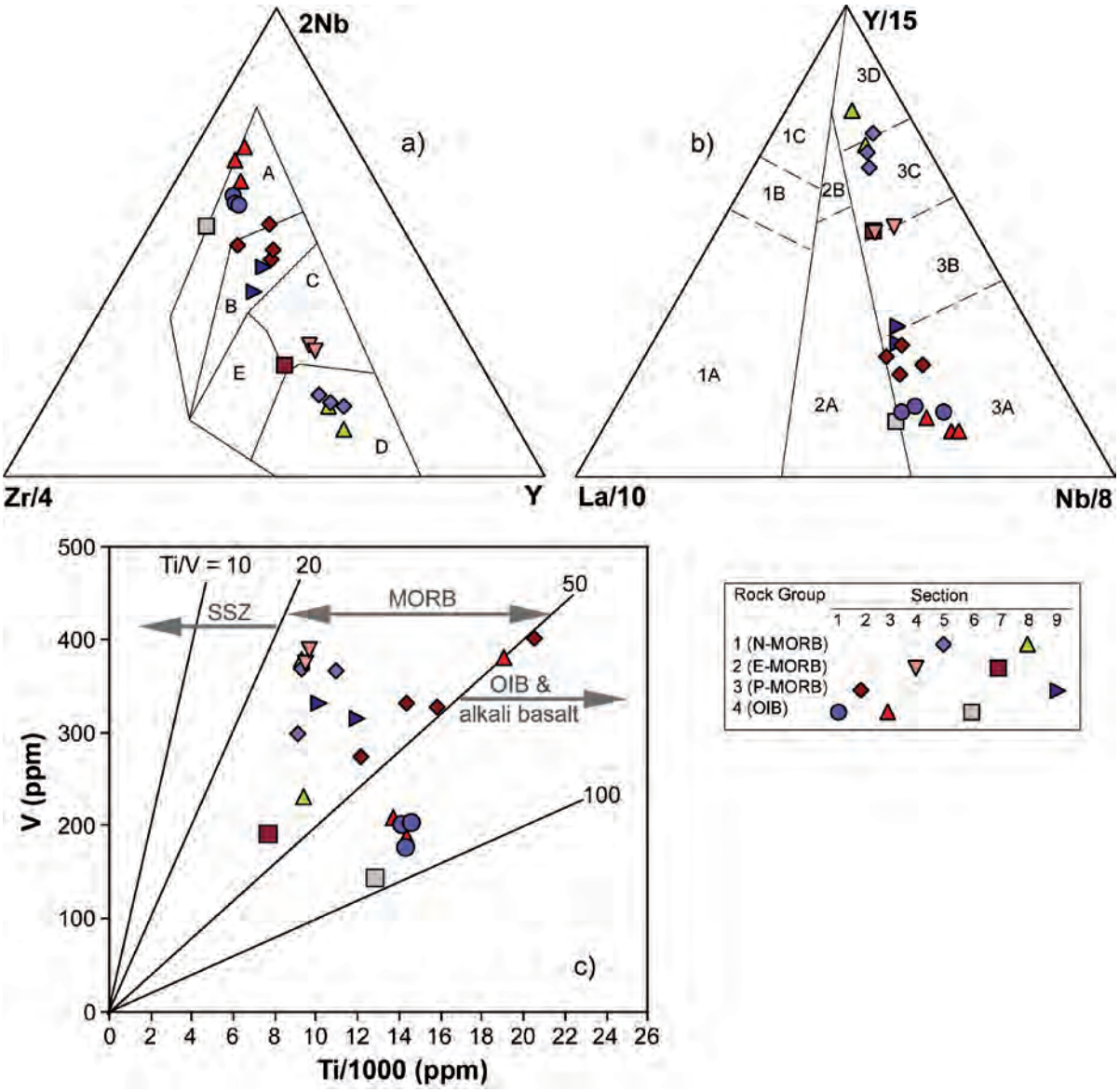


Fig. 7 - a) Zr/4-Y-2Nb (Meschede, 1986); b) La/10-Nb/8-Y/15 (Cabanis and Lécolle, 1989); c) V vs. Ti/1000 (Shervais, 1982) discrimination diagrams for volcanic rocks from the Izmir-Ankara Mélange. Fields in Fig. 7a: A- within-plate alkali basalts; B- within-plate alkali basalts and within-plate tholeiites; C- enriched mid-ocean ridge basalts; D- normal mid-ocean ridge basalts; E- within-plate tholeiites and volcanic-arc basalts. Fields in Fig.7b: 1A- calc-alkaline basalts; 1B- overlapping of 1A and 1B; 1C- volcanic arc tholeiites; 2A- continental basalts; 2B- backarc basalts; 3A- within-plate alkali basalts; 3B and 3C- enriched mid-ocean ridge basalts (3B more enriched than 3C); 3D- normal mid-ocean ridge basalts.

The age ranges from the published biostratigraphical data indicate gaps in Early Jurassic and late Early Cretaceous (see Göncüoglu et al., 2010). Moreover, Late Triassic and Middle Jurassic findings were restricted to a limited number of samples. This scarcity of biostratigraphical data has even been used by some authors (e.g., Rojay, 2013) for denying a pre-Middle Jurassic spreading phase within the Izmir-Ankara Ocean. The new radiolarian findings of this study provide additional evidence on Late Triassic (late Norian), Middle-Late Jurassic and late Early Cretaceous pelagic deposition associated with basaltic volcanism in the oceanic basin.

## REMARKS AND CONCLUSIONS

One of the crucial points in the history of the Izmir-Ankara oceanic branch regards its opening age. The earliest suggestion, from Görür et al. (1983), dominated the geodynamic models and still has some followers (e.g., Rojay, 2013). Görür et al. (1983), postulated that this oceanic branch opened not earlier then late Early Liassic.

It is noteworthy that the pelagic sediments (Bragin and Tekin, 1996), collected in cherty blocks of the mélange, gave a late Norian age (Late Triassic). Moreover, a cherty bed intercalated in the pelagic limestones and associated to the E-MORB basalts (Tekin et al., 2002; Göncüoglu et al., 2010) indicated an early late Carnian age (Late Triassic). These data could suggest that the oceanization process of the Izmir-Ankara Ocean was active from the Late Triassic.

The new Late Triassic radiolarian age (Section 6: late Norian) obtained in this study is from Group 4 basaltic rocks with OIB character. Their significant HREE fractionation may indicate an enriched source and may suggest the involvement of plume-type geochemical components.

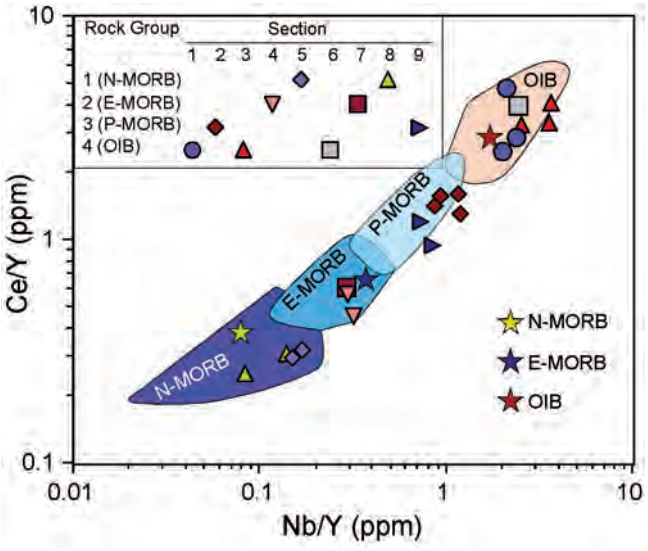


Fig. 8 - Ce/Y vs. Nb/Y diagram for volcanic rocks from the Izmir-Ankara Mélange. The compositions of normal mid-ocean ridge basalt (N-MORB), enriched mid-ocean ridge basalt (E-MORB), and ocean-island basalt (OIB) are from Sun and McDonough (1989). The compositional variations for N-MORBs, E-MORBs, P-MORBs (plume-type MORB) and alkaline OIB from the Albanian (Bortolotti et al., 2004, 2006; Tashko et al., 2009), Hellenides (Photiades et al., 2003; Saccani et al., 2008; Saccani and Photiades, 2005; Bortolotti et al., 2008; Chiari et al., 2012), Turkish (Tankut et al., 1998), Iranian (Arvin and Robinson, 1994; Saccani et al., 2010, 2013a, b), and Oman (Lapierre et al., 2004; Chauvet et al., 2011) ophiolites are shown for comparison. Note that literature data reported for comparison refer to ophiolitic units where the different rock-types listed above crop out in association.

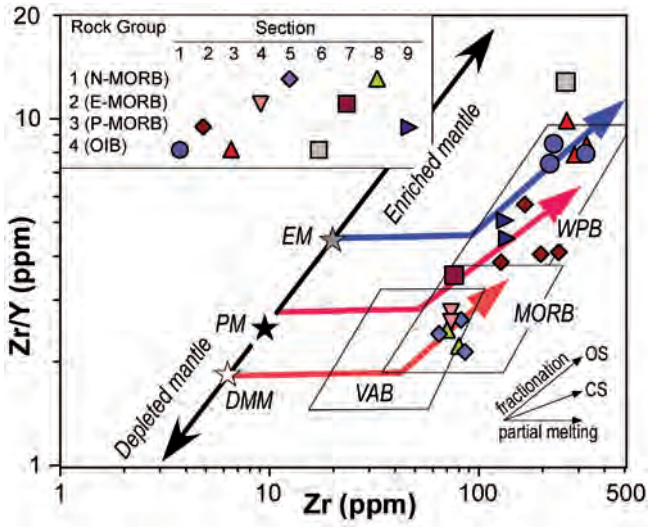


Fig. 9 - Zr/Y vs. Zr diagram for volcanic rocks from the Izmir-Ankara Mélange (modified from Pearce and Norry, 1979). Possible fractionation trends for the subalkaline, transitional, and alkaline rocks are indicated by arrows. DMM- depleted MORB mantle; PM- primitive mantle; EM:-enriched mantle; OS- open-system fractionation; CS- closed-system fractionation; MORB- mid-ocean ridge basalt; VAB- volcanic arc basalt; WPB-within-plate basalt.

In previous studies Tekin et al. (2002) and Göncüoglu et al. (2010) suggested that the Late Triassic volcanism points to an initial stage of oceanic crust formation by continental rifting with or without the involvement of a mantle plume.

The recent finding supports the deeper mantle origin but favours a limited lithospheric extension. However, the absence of lower crustal contamination constraints their generation during the initial opening and suggests a more advanced phase.

In the present study the E-MORB type rocks were found in two sections of Cretaceous age (Section 4: middle late Barremian-early early Aptian and Section 7: Valanginian to middle Aptian-early Albian).

The oldest N-MORB lavas from the western IAESB were previously dated as Middle to Late Jurassic (e.g., Göncüoglu et al., 2006). This datum is confirmed by our finding of Late Jurassic volcanic rocks in the central IAESB (Section 5: early-early late Tithonian) and demonstrates, together with Cretaceous ages that the ocean spreading was in progress during Mid-Late Mesozoic times. Futhermore our other new findings partially fill the gap during late Early Cretaceous (see Göncüoglu et al., 2010). In fact the radiolarian cherts associated to the N-MORB of Section 8 indicated a late Valanginian-early Barremian age.

Yet, no Early Jurassic basalts were found in the oceanic assemblages of this Neotethyan oceanic branch. Hence, the development of IAESB during the Early Jurassic remains a critical question.

OIB type volcanic rocks are common in the IAESB. In the present study, OIB-type rocks of Late Jurassic (Section 3: middle-late Oxfordian to late Kimmeridgian-early Tithonian) and Early Cretaceous ages (Section 1: late Valanginian to late Hauterivian) are interpreted as derived from partial melting of plume-type enriched mantle source(s). Our data do not allow to discriminate if the plume-type enriched mantle source was associated to mantle plume activity or if this enriched geochemical feature was inherited from previous mantle plume activity in the same area. However, lacking any direct evidence supporting the existence of mantle plume activity, we favour the hypothesis that the enriched nature of the mantle source(s) was likely inherited from a previous stage.

This finding is in good accordance with the previous data from the western IAESB (e.g., Göncüoglu et al., 2010) and from the Neotethyan suture belts in the Eastern Mediterranean (e.g., Robertson, 2002; Bortolotti and Principi, 2005).

In the present work we document, the occurrence of OIB-type rocks of late Norian age (Section 6) and of rocks showing different geochemical affinities (N-, E-, P-MORBs and OIB) generated in the same time span (Middle-Late Jurassic - Early Cretaceous). As shown in the previous chapters, N-MORBs are compatible with composition of melts generated by partial melting of a depleted MORB mantle source. In contrast, OIBs are compatible with partial melting of an enriched-type mantle source. E-MORBs may have derived from mantle source slightly enriched with respect to a DMM source, whereas P-MORBs (Section 9: not dated and Section 2: early-middle Bajocian to late Bathonian-early Callovian age) are compatible with melts generated from a mantle source significantly enriched, compared to DMM.

Therefore, we can postulate that different mantle sources existed and interacted from Middle Jurassic to Early Cretaceous. Partial melting of an OIB-type enriched source led to the production of the alkaline basalts, whereas partial melting of a DMM heterogeneously modified by OIB-type components produced both P- and E-MORBs. In contrast, partial melting of a pure DMM led to the produc-

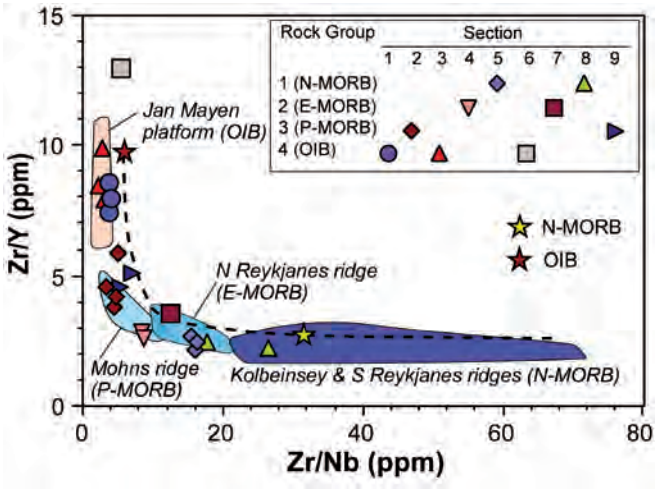


Fig. 10 - Zr/Y vs. Zr/Nb diagram for volcanic rocks from the Izmir-Ankara Mélange. The compositions of modern normal mid-ocean ridge basalt (N-MORB) and ocean-island basalt (OIB) are from Sun and McDonough (1989). The compositional variation for ocean-floor basalts erupted in the North Atlantic Ocean is shown for comparison (data from Hanan et al., 2000). The dashed line represents the mixing curve calculated using the OIB and N-MORB end members.

tion of N-MORBs (Section 8: late Valanginian-early Barremian age). Furthermore, other N-MORBs (Section 5: early-early late Tithonian) may have a light OIB-type compositional influence, but the incompatible element general composition indicates that such an OIB-type influence was negligible.

Some of the late Early Cretaceous OIB's found in the central IEASB overlap temporally with the E-MORB's. This may indicate a second period of enriched mantle that could be generated by a number of different tectonic events including lithospheric extension, slab break-of, slab roll-back etc. Previous data on the earliest ages related to supra-subduction type volcanism and formation of metamorphic sole indicated early Late Cretaceous (e.g., Üner 2010), therefore the intra-oceanic decoupling within the Izmir-Ankara Ocean was considered as pre-Late Cretaceous. This age could not be verified in this study, since in contrast to the western part of the IAESB, none of the basalt samples collected from the central part yielded supra-subduction characteristics. This is also in contradiction with respect to the very recent finding of early Middle Jurassic (Celik et al., 2011) metamorphic sole in the sampled area.

## AKNOWLEDGMENTS

The Italian Ministry of Education, University and Research (MIUR) is acknowledged for the financial support. Special thanks go to Michele Marroni and Paulian Dumitrica for their constructive reviews of this paper and to Benedetta Treves for language review. Special thanks go to Mirella Bonora (Ferrara University) for her support with analytical techniques.

Radiolarian micrographs were taken with a Philips XL20 of the Ivalsa Institute, (CNR) by Simona Lazzeri.

## REFERENCES

Aldanmaz E., Yaliniz M.K., Guctekin A. and Göncüoglu M.C., 2008. Geochemical characteristics of mafic lavas from the Neotethyan ophiolites in western Turkey: implications for heterogeneous source contribution during variable stages of ocean crust generation. Geol. Mag., 145: 37-54.

Allahyari K., Saccani E., Pourmoafi M., Beccaluva L. and Masoudi F., 2010. Petrology of mantle peridotites and intrusive mafic rocks from the Kermanshah ophiolitic complex (Zagros belt, Iran): Implications for the geodynamic evolution of the Neo-Tethyan oceanic branch between Arabia and Iran. Ofioliti, 35: 71-90.

Allègre C.J. and Minster J.F., 1978. Quantitative models of trace element behaviour in magmatic processes. Earth Planet. Sci. Lett., 38: 1-25.

Altiner D., Koçyiğit A., Farinacci A., Nicosia U. and Conti M.A., 1991. Jurassic-Lower Cretaceous stratigraphy and paleogeographic evolution of the southern part of north-western Anatolia (Turkey). Geol. Romana, 27: 13-80.

Arvin M. and Robinson P., 1994. The petrogenesis and tectonic setting of lavas from the Baft ophiolitic mélange, soutwest of Kerman, Iran. Can. J. Earth Sci., 31: 824-834.

Bailey E.B. and McCallien W.J., 1953. Serpentinite lavas, the Ankara Mélange, and the Anatolian Thrust. Trans. Roy. Soc. Edin., 57: 403-442.

Bak M., 1996. Cretaceous radiolaria from Niedzica Succession of the Pieniny Klippen Belt in Polish Carpathians. Acta Palaeont. Polonica, 41 (1): 91-110.

Bak M., 1999. Cretaceous radiolarian zonation in the Polish part of the Pieniny Klippen Belt (Western Carpathians). Geol. Carpath., 50 (1): 21-31.

Bandini A.N., Baumgartner P.O., Flores K., Dumitrica P. and Jackett S.J., 2011. Early Jurassic to early Late Cretaceous radiolarians from the Santa Rosa accretionary complex (northwestern Costa Rica). Ofioliti, 31 (1): 1-35.

Baumgartner P.O., O'Dogherty L., Goričan Š., Dumitrica-Jud R., Dumitrica P., Pillevuit A., Urquhart E., Matsuoka A., Danelian T., Bartolini A.C., Carter E.S., De Wever P., Kito N., Marcucci M. and Steiger T.A., 1995a. Radiolarian catalogue and systematics of Middle Jurassic to Early Cretaceous Tethyan genera and species. In: P.O. Baumgartner et al., (Eds.), Middle Jurassic to Lower Cretaceous Radiolaria of Tethys: occurrences, systematics, biochronology. Mém. Géol., Lausanne, 23: 37-685.

Baumgartner P.O., Bartolini A.C., Carter E.S., Conti M., Cortese G., Danelian T., De Wever P., Dumitrica P., Dumitrica-Jud R., Goričan Š., Guex J., Hull D.M., Kito N., Marcucci M., Matsuoka A., Murchey B., O'Dogherty L., Savary J., Vishnevskaya V., Widz D. and Yao A., 1995b. Middle Jurassic to Early Cretaceous Radiolarian biochronology of Tethys based on Unitary Associations. In: P.O. Baumgartner et al., (Eds.), Middle Jurassic to Lower Cretaceous radiolaria of Tethys: occurrences, systematics, biochronology, Mém. Géol., Lausanne, 23: 1013-1048.

Baumgartner P.O., Bjørklund K.R., Caulet J.P., De Wever P., Kellogg D., Labracherie M., Nakaseko K., Nishimura A., Schaff A., Schimdt-Effing R. and Yao A., 1981. Eurorad II, 1980. Second European meeting of radiolarian paleontologists: current research on Cenozoic and Mesozoic radiolarians. Eclog. Geol. Helv., 74 (3): 1027-1061.

Boccaletti M., Bortolotti V. and Sagri M., 1966. Ricerche sulle ofioliti delle catene alpine: I. Osservazioni sull'Ankara Mélange nelle zona di Ankara. Boll. Soc. Geol. It., 85: 485-508.

Bortolotti V. and Principi G., 2005. Tethyan ophiolites and Pangea break-up. Isl. Arc., 14: 442-470.

Bortolotti V. and Sagri M., 1968. Ricerche sulle ofioliti delle catene alpine. 4- Osservazioni sull'età e la giacitura delle ofioliti tra Smirne ed Erzurum (Turchia). Boll. Soc. Geol. It., 87: 661-666.

Bortolotti V., Chiari M., Kodra A., Marcucci M., Marroni M., Mustafa F., Prela M., Pandolfi L., Principi G. and Saccani E., 2006. Triassic MORB magmatism in the southern Mirdita zone (Albania). Ofioliti, 31: 1-9.

Bortolotti V., Chiari M., Kodra A., Marcucci M., Mustafa F., Principi G. and Saccani E., 2004. New evidence for Triassic MORB magmatism in the northern Mirdita Zone ophiolites (Albania). Ofioliti, 29: 243-246.

Bortolotti V., Chiari M., Marcucci M., Photiades A., Principi G. and Saccani E., 2008. New geochemical and age data on the ophiolites from the Othrys area (Greece): Implication for the Triassic evolution of the Vardar Ocean. Ofioliti, 33: 135-151.

Bragin N.Yu., 2007. Late Triassic radiolarians of southern Cyprus. Paleont. J., 41 (10): 951-1029.

Bragin N.Yu. and Tekin U.K., 1996. Age of radiolarian-chert blocks from the Senonian ophiolitic mélange (Ankara, Turkey). Isl. Arc, 5: 114-122.

Cabanis B. and Lécolle M., 1989. Le diagramme La/10, Y/15, Nb/8: un outil pour la discrimination des séries volcaniques et la mise en évidencedes processus de mélange et/ou contamination crustale. C.R. Acad. Sci. Paris, 309: 2023-2029.

Carter E.S., 1993. Biochronology and paleontology of uppermost Triassic (Rhaetian) radiolarians, Queen Charlotte Islands, British Columbia, Canada. Mém. Géol., Lausanne, 11: 1-175.

Cater J.M.L., Hanna S.S, Ries A.C, and Turner P., 1991.Tertiary evolution of the Sivas Basin, central Turkey. Tectonophysics, 195: 29-46.

Celik S., 2010. Taxonomy and biostratigraphy of Jurassic-Early Cretaceous radiolarian fauna of the pelagic deposits in Izmir-Ankara-Erzincan suture complex, NE and SW Çankırı, northern Turkey. Hacettepe Univ., M.Sci. Thesis, 1-133 (unpublished) (in Turkish with English abstract).

Celik O.M., Marzoli A., Marschik R., Chiaradia M., Neubauer F. and Öz I., 2011. Early-Middle Jurassic intra-oceanic subduction in the ˙Izmir-Ankara-Erzincan Ocean, Northern Turkey. Tectonophysics, 509: 120-134.

Cemen I., Göncüoğlu M.C., Erler A., Kozlu H. and Perinçek D., 1993. Indentation tectonics and associated lateral extrusion in East, Southeast and Central Anatolia: Geol. Soc. Am., Progr. Abstr., p: A116-117

Chauvet F., Lapierre H., Maury R. C., Bosch D., Basile C., Cotten J., Brunet P. and Campillo S., 2011. Triassic alkaline magmatism of the Hawasina Nappes: Post-breakup melting of the Oman lithospheric mantle modified by the Permian Neotethyan Plume. Lithos, 122: 122-136.

Chiari M., Bortolotti V., Marcucci M., Photiades A., Principi G. and Saccani E., 2012. Radiolarian biostratigraphy and geochemistry of the Koziakas Massif ophiolites (Greece). Bull. Soc. Géol. France, 183: 289-309.

Chiari M., Cobianchi M. and Picotti V., 2007. Integrated stratigraphy (radiolarians and calcareous nannofossils) of the Middle to Upper Jurassic Alpine radiolarites (Lombard Basin, Italy): Constraints to their genetic interpretation. Palaeo. Palaeo. Palaeo., 249: 233-270.

Dangerfield A., Harris R., Sarifakioğlu E. and Dilek Y., 2011. Tectonic evolution of the Ankara Mélange and associated Eldivan ophiolite near Hançili, central Turkey. Melanges: Processes of formation and societal significance: Geol. Soc. Am. Spec. Pap., 480: 143-169.

Dercourt J., Zonenshain L.P., Ricou L.E., Kazmin V.G., Le Pichon X., Knipper A.L., Grandjacquet C, Sbortshikov I.M., Geyssant J., Lepvrier C., Pechersky D.H., Boulin J., Sibuet J.C., Savostin L.A., Sorokhtin O., Westphal M., Bazhenov M.L., Lauer J.P. and Biju-Duval B., 1986. Geological evolution of the Tethys belt from the Atlantic to the Pamirs since the Lias. In: J. Aubouin, X. Le Pichon and A.S. Monin (Eds.), Evolution of the Tethys. Tectonophysics, 123: 241-315.

De Wever P., 1982. Radiolaires du Trias et du Lias de la Téthys (Systématique, Stratigraphie). Soc. Géol. Nord, 7: 1-600.

Dilek Y., Thy P., Hacker B. and Grundvig S., 1999. Structure and petrology of Tauride ophiolites and mafic dike intrusions (Turkey): Implications for the Neo-Tethyan Ocean. Geol. Soc. Am. Bull., 111: 1192-1216.

Dumitrica P., 1970. Cryptocephalic and cryptothoracic Nassellaria in some Mesozoic deposits of Romania. Rev. Roum. Géol., Géophys. Géogr. (série Géologie), 14 (1): 45-124.

Dumitrica P. and Dumitrica-Jud R., 1995. *Aurisaturnalis carinatus* (Foreman), an example of phyletic gradualism among Saturnalid-type radio larians. Rev. Micropal., 38 (3): 195-216.

Dumitrica P., Immenhauser A. and Dumitrica-Jud R., 1997. Mesozoic radiolarian biostratigraphy from Masirah Ophiolite, Sultanate of Oman Part I: Middle Triassic, Uppermost Jurassic and Lower Cretaceous Spumellarians and multisegmented Nassellarians. Bull. Nat. Mus. Nat. Sci., Taiwan, 9: 1-106.

Erdogan B., Akay C. and Ugur M.S., 1996. Geology of the Yozgat region and evolution of the collisional Çankırı basin, Intern. Geol. Rev., 38: 788-806.

Floyd P.A., Göncüoglu M.C., Winchester J.A. and Yalınız M.K., 2000. Geochemical character and tectonic environment of Neotethyan ophiolitic fragments and metabasites in the Central Anatolian Crystalline Complex, Turkey. In: E. Bozkurt, J. Winchester and J.A. Piper (Eds.), Tectonics and magmatism in Turkey and the surrounding area. Geol. Soc. London Spec. Publ., 173: 183-202.

Gökten E. and Floyd P.A., 2007. Stratigraphy and geochemistry of pillow basalts within the ophiolitic mélange of the Izmir-Ankara-Erzincan suture zone: implications for the geotectonic character of the northern branch of Neotethys. Int. J. Earth Sci. (Geol. Rundsch.), 96: 725-741.

Göncüoglu M.C., 1992. Structural and stratigraphical framework of the Central Anatolian Tertiary basins. In: E. Sirel and E. Yazgan (Eds.), Introduction to the Early Paleogene of the Haymana-Polatlı Basin, Field Trip Guidebook. General Dir. Mineral Res. Explor., Ankara, p. 1-11.

Göncüoglu M.C., 2011. Geology of the Kütahya-Bolkardağ Belt. Min. Res. Explor. Bull., 142: 223-277.

Göncüoglu M.C., Dirik K. and Kozlu H., 1997. General characteristics of pre-Alpine and Alpine Terranes in Turkey: Explanatory notes to the terrane map of Turkey. Ann. Géol. Pays Hellén., 37: 515-536.

Göncüoglu M.C., Gürsu S., Tekin U.K. and Köksal S., 2008. New data on the evolution of the Neotethyan oceanic branches in Turkey: Late Jurassic ridge spreading in the Intra-Pontide branch. Ofioliti, 33 (2): 153-164.

Göncüoglu M.C., Marroni M., Sayit K., Tekin U.K., Pandolfi L. and Ellero A., 2012. The Ayli Dağ ophiolite sequence (Central-Northern Turkey): a fragment of Middle Jurassic oceanic lithosphere within the Intra-Pontide Suture Zone. Ofioliti, 37 (2): 77-92.

Göncüoglu M.C., Sayit K. and Tekin U.K., 2010. Oceanization of the northern Neotethys: Geochemical evidence from ophiolitic mélange basalts within the İzmir-Ankara suture belt, NW Turkey. Lithos, 116: 175-187.

Göncüoglu M.C., Tekin U.K. and Turhan N., 2001. Geological meaning of the Late Carnian basalts blocks with radiolarites within the Late Cretaceous Central Sakarya ophiolitic complex (NW Anatolia). Jeo 2000 Proceed., CD-54-6: 6.

Göncüoglu M.C., Turhan N., Sentürk K., Özcan A. and Uysal S., 2000. A geotraverse across NW Turkey: tectonic units of the Central Sakarya region and their tectonic evolution. In: E. Bozkurt, J Winchester and J.A. Piper (Eds.), Tectonics and magmatism in Turkey and the surrounding area. Geol. Soc. London Spec. Publ., 173: 139-161.

Göncüoglu M.C., Yaliniz K. and Tekin U.K., 2006. Geochemistry, tectono-magmatic discrimination and radiolarian ages of basic extrusives within the Izmir-Ankara Suture Belt (NW Turkey): time constraints for the Neotethyan evolution. Ofioliti, 31: 25-38.

Görür N., Sengör A. M.C., Akkök R. and Yilmaz Y., 1983. Sedimentological evidence for the opening of the northern branch of Neo-Tethys in the Pontides. (Turkish with English abstract), Bull. Geol. Soc. Turk., 26: 11-19.

Gülyüz E, Kaymakci N., Meijers M.J.M., van Hinsbergen D.J.J., Lefebvre C.,Vissers R.L.M., Bart W.H., Hendriks B.W.H. and Peynircioglu A.A., 2012. Late Eocene evolution of the Çiçekdağı Basin (central Turkey): syn-sedimentary compression during microcontinent-continent collision in central Anatolia. Tectonophysics, 602: 286-299.

Hanan B.B., Blichert-Toft J., Kingsley R. and Schilling J.G., 2000. Depleted Iceland mantle plume geochemical signature: Artifact of multicomponent mixing? Geochem. Geophys. Geosyst., 1 (4): 1-19.

Jackson M.L., 1958. Soil chemical analysis. Prentice-Hall, 498 pp.

Kocyigit A., Türkmenoglu A., Beyhan A., Kaymakçı N. and Akyol E., 1995. Post-collisonal tectonics of Eskişehir-Ankara-Çankırı segment of Izmir-Ankara-Erzincan Suture Zone. Turk. Ass. Petrol. Geol. Bul., 6: 69-87.

Kaymakci N., Duermeijer C.E., Langereis C., White S.H. and van Dijk P.M., 2003. Paleomagnetic evolution of the Çankırı Basin (Central Anatolia, Turkey: Implication for oroclinal bending due to indentation. Geol. Mag., 140: 343-355.

Köksal S. and Göncüoglu C., 2008. Sr and Nd isotopic characteristics of some S-, I- and A-type granitoids from Central Anatolia. Turk. J. Earth Sci., 17: 111-127.

Lachance G.R. and Trail R.J., 1966. Practical solution to the matrix problem in X-ray analysis. Can. Spectrosc., 11: 43-48.

Lapierre H., Samper A., Bosch D., Maury R.C., Béchennec F., Cotten J., Demant A., Brunet P., Keller F. and Marcoux J., 2004. The Tethyan plume: geochemical diversity of Middle Permian basalts from the Oman rifted margin. Lithos, 74: 167-198.

Meschede M., 1986. A method of discriminating between different types of mid-ocean ridge basalts and continental tholeiites with the Nb-Zr-Y diagram. Chem. Geol., 56: 207-218.

Moix P., Beccaletto L., Kozur H.W., Hochard C., Rosselet F. and Stampfli G.M., 2008. A new classification of the Turkish terranes and sutures and its implication for the paleotectonic history of the region. Tectonophysics, 451: 7-39.

O'Dogherty L., 1994. Biochronology and paleontology of Mid-Cretaceous radiolarians from Northern Apennines (Italy) and Betic Cordillera (Spain). Mém. Géol., Lausanne, 21: 1-415.

O'Dogherty L., Carter E.S., Dumitrica P., Goričan Š., De Wever P., Hungerbühler A., Bandini A.N. and Takemura A., 2009a. Catalogue of Mesozoic radiolarian genera. Part 1: Triassic. Geodiversitas, 31: 213-270.

O'Dogherty L., Carter E.S., Dumitrica P., Goričan Š., De Wever P., Bandini A.N., Baumgartner P.O. and Matsuoka A., 2009b. Catalogue of Mesozoic radiolarian genera. Part 2: Jurassic-Cretaceous. Geodiversitas, 31: 271-356.

Okay A.I. and Göncüoglu M.C., 2004. The Karakaya Complex: A review of data and concepts. Turk. J. Earth Sci., 13: 75-95.

Okay A.I. and Tüysüz O., 1999. Tethyan sutures of northern Turkey. In: B. Durand, L. Jolivet, F Horváth and M. Séranne (Eds.), The Mediterranean Basin: Tertiary extension within the Alpine orogen. Geol. Soc. London Spec. Publ., 156: 475-515.

Okay A.I., Satir M. and Siebel W., 2006. Pre-Alpide Palaeozoic and Mesozoic orogenic events in the Eastern Mediterranean region. In: D.G. Gee and R.A. Stephenson (Eds.), European lithosphere dynamics. Geol. Soc. London Mem., 32: 389-405.

Önen A.P., 2003. Neotethyan ophiolitic rocks of the Anatolides of NW Turkey and comparison with Tauride ophiolites. J. Geol. Soc. London, 160: 947-962.

Parlak O., Çolakoglu A., Dönmez, C., Sayak H., Yildirim N., Türkel A. and Odabasi I., 2012. Geochemistry and tectonic significance of ophiolites in northeastern Anatolia along the Izmir-Ankara-Erzincan Suture Zone. In: A.H.F. Robertson, O. Parlak and U.C. Unlugenc (Eds.), Geological development of Anatolia and the easternmost Mediterranean Region. Geol. Soc. London Spec. Publ., 37: doi: 10.1144/SP372.7

Pearce J.A., 1982. Trace element characteristics of lavas from destructive plate boundaries. In: R.S. Thorpe (Ed.), Andesites. John Wiley and Sons, New York, p. 525-548.

Pearce J.A. and Norry M.J., 1979. Petrogenetic implications of Ti, Zr, Y, and Nb variations in volcanic rocks. Contrib. Miner. Petrol., 69: 33-47.

Pessagno E.A. and Newport L.A., 1972. A technique for extracting Radiolaria from radiolarian chert. Micropaleontology, 18: 231-234.

Photiades A., Saccani E. and Tassinari R., 2003. Petrogenesis and tectonic setting of volcanic rocks from the Subpelagonian ophiolitic mélange in the Agoriani area (Othrys, Greece). Ofioliti, 28: 121-135.

Robertson, A.H.F., 2000. Mesozoic-Tertiary tectonic-sedimentary evolution of a south Tethyan oceanic basin and its margins in southern Turkey. In: E. Bozkurt, J.A. Winchester and J.D. Piper (Eds.), Tectonics and magmatism in Turkey and the surrounding area. Geol. Soc. London Spec. Publ., 173: 43-82.

Robertson A.H.F., 2002. Overview of the genesis and emplacement of Mesozoic ophiolites in the Eastern Mediterranean Tethyan region. Lithos, 65: 1-67.

Robertson A.H.F., 2004. Development of concepts concerning the genesis and emplacement of Tethyan ophiolites in the East Mediterranean and Oman regions. Earth Sci. Rev., 66: 331-387.

Robertson A.H.F., Dixon J.E., Brown S. Collins, A., Morris, A., Pickett E.A., Sharp I. and Ustaömer T., 1996. Alternative tectonic models for the Late Palaeozoic-Early Tertiary development of Tethys in the Eastern Mediterranean region. In: A. Morris and D.H. Tarling (Eds.), Palaeomagnetism and tectonics of the Mediterranean region. Geol. Soc. London Spec. Publ., 105: 239-63.

Robin C., Goričan Š., Guillocheau F., Razin P., Dromart G. and Mosaffa H., 2010. Mesozoic deep-water carbonate deposits from the southern Tethyan passive margin in Iran (Pichakun nappes, Neyriz area): biostratigraphy, facies sedimentology and sequence stratigraphy. In: P. Leturmy and C. Robin (Eds.), Tectonic and stratigraphic evolution of Zagros and Makran during the Mesozoic-Cenozoic. Geol. Soc. London Spec. Publ., 330: 179-210.

Rojay B., 2013. Tectonic evolution of the Cretaceous Ankara Ophiolitic Mélange during the Late Cretaceous to pre-Miocene interval in Central Anatolia, Turkey. J. Geodyn., 65: 66-81.

Rojay B., Yaliniz M.K. and Altiner D., 2001. Tectonic implications of some Cretaceous pillow basalts from the North Anatolian Ophiolitic Mélange (Central Anatolia-Turkey) to the evolution of Neotethys. Turk. J. Earth Sci., 10: 93-102.

Saccani E. and Photiades A., 2005. Petrogenesis and tectono-magmatic significance of volcanic and subvolcanic rocks in the Albanide-Hellenide ophiolitic mélanges. Isl. Arc, 14: 494-516.

Saccani E., Allahyari K., Beccaluva L. and Bianchini G., 2013a. Geochemistry and petrology of the Kermanshah ophiolites (Iran): Implication for the interaction between passive rifting, oceanic accretion, and plume-components in the Southern Neo-Tethys Ocean. Gondwana Res., 24: 392-411.

Saccani E., Azimzadeh Z., Dilek Y. and Jahangiri A., 2013b. Geochronology and petrology of the Early Carboniferous Misho Mafic Complex (NW Iran), and implications for the melt evolution of Paleo-Tethyan rifting in Western Cimmeria. Lithos, 162-163: 264-278.

Saccani E., Delavari M., Beccaluva L. and Amini S.A., 2010. Petrological and geochemical constraints on the origin of the Nehbandan ophiolitic complex (eastern Iran): Implication for the evolution of the Sistan Ocean. Lithos, 117: 209-228.

Saccani E., Photiades A., Santato A. and Zeda O., 2008. New evidence for supra-subduction zone ophiolites in the Vardar Zone from the Vermion Massif (northern Greece): Implication for the tectono-magmatic evolution of the Vardar oceanic basin. Ofioliti, 33: 65-85.

Sayit K., Tekin U.K. and Göncüoglu M.C., 2011. Early-Middle Carnian radiolarian cherts within the Eymir Unit, Central Turkey: Constraints for the age of the Palaeotethyan Karakaya Complex. J. Asian Earth Sci., 42: 398-407.

Schmid S.M., Bernoulli D., Fügenschuh B., Matenco L., Schefer S., Schuster R., Tischler M. and Ustaszewski K., 2008. The Alpine-Carphatian-Dinaridic orogenic system: correlation and evolution of tectonic units. Swiss J. Geosci., 101:139-183.

Sengör A.M.C. and Yilmaz Y., 1981. Tethyan evolution of Turkey: a plate tectonic approach. Tectonophysics, 75: 181-241.

Shervais J.W., 1982. Ti-V plots and the petrogenesis of modern ophiolitic lavas. Earth Planet. Sci. Lett., 59: 101-118.

Stampfli G.M. and Borel G.D., 2002. A plate tectonic model for the Palaeozoic and Mesozoic constrained by dynamic plate boundaries and restored synthetic oceanic isochrones: Earth Planet. Sci. Lett., 169: 17-33.

Sugiyama K., 1997. Triassic and Lower Jurassic radiolarian biostratigraphy in the siliceous claystone and bedded chert units of the southeastern Mino Terrane, Central Japan. Bull. Mizunami Fossil Mus., 24: 79-193.

Sun S.S. and McDonough W.F., 1989. Chemical and isotopic-systematics of oceanic basalts: implications for mantle composition and processes. In: A.D. Saunders and M.J. Norry (Eds.), Magmatism in the ocean basins. Geol. Soc. London Spec. Publ., 42: 313-345.

Tankut A., Dilek Y. and Onen P., 1998. Petrology and geochemistry of the Neo-Tethyan volcanism as revealed in the Ankara mélange, Turk. J. Volcan. Geotherm. Res., 85: 265-284.

Tashko A., Mascle G.H., Muceku B. and Lapierre H., 2009. Nd, Pb isotope and trace element signatures of the Triassic volcanism in Albania. The relationship to the NeoTethys opening. Alban. J. Nat. Techn. Sci., 1 (21): 3-23.

Tekin U.K., 1999. Biostratigraphy and systematics of Late Middle to Late Triassic radiolarians from the Taurus Mountains and Ankara region, Turkey. Geol. Paläont. Mitt. Innsbruck, Sonderb., 5: 1-296.

Tekin U.K., 2002. Late Triassic (late Norian-Rhaetian) radiolarians from the Antalya Nappes, central Taurides, southern Turkey. Riv. It. Paleont. Strat., 108: 415-440.

Tekin U.K. and Göncüoglu MC., 2007. Discovery of the oldest (Upper Ladinian to Middle Carnian) radiolarian assemblages from the Bornova Flysch Zone in western Turkey: Implications for the evolution of the Neotethyan Izmir-Ankara Ocean. Ofioliti, 32: 131-150.

Tekin U.K. and Göncüoglu M.C., 2009. Late Middle Jurassic (late Bathonian-early Callovian) radiolarian cherts from the Neotethyan Bornova Flysch Zone, Spil Mountains, Western Turkey. Stratigr. Geol. Correl., 17: 298-308.

Tekin U.K., Göncüoglu M.C., and Turhan N., 2002. First evidence of Late Carnian radiolarian fauna from the Izmir-Ankara Suture Complex, Central Sakarya, Turkey: implications for the opening age of the Izmir-Ankara branch of Neotethys. Geobios, 35: 127-135.

Tekin U.K., Göncüoglu M.C and Uzuncimen S., 2012. Radiolarian assemblages of Middle and Late Jurassic to early Late Cretaceous (Cenomanian) ages from an olistolith record pelagic deposition within the Bornova Flysch Zone in western Turkey. Bull. Soc. Géol. France, 183 (4): 307-318.

Üner T. 2010. Petrology of Eldivan and Ahlat (Çankırı) ophiolites. Hacettepe Univ., Ph.D. Thesis, p. 1-185 (unpublished) (in Turkish with English abstract).

Winchester J.A. and Floyd P.A., 1977. Geochemical discrimination of different magma series and their differentiation products using immobile elements. Chem. Geol., 20: 325-344.

Workman R.K. and Hart S.R., 2005. Major and trace element composition of the depleted MORB mantle (DMM). Earth Planet. Sci. Lett., 231: 53-72.

Yaliniz M.K., Floyd P.A. and Göncüoglu, M.C., 1996, Supra-subduction zone ophiolites of Central Anatolia: geochemical evidence from the Sarıkaraman Ophiolite, Aksaray, Turk. Mineral. Mag., 60: 697-710.

Yaliniz K., Göncüoglu M.C. and Floyd P.A., 2000a, Geochemistry of volcanic rocks from the Çicekdağ Ophiolite, Central Anatolia, Turkey, and their inferred tectonic setting within the northern branch of the Neotethyan ocean. In: E. Bozkurt, J. Winchester and J.A. Piper (Eds.), Tectonics and magmatism in Turkey and the surrounding area. Geol. Soc. London Spec. Publ., 173: 203-218.

Yaliniz M.K., Göncüoglu M.C. and Özkan-Altiner S., 2000b. Formation and emplacement ages of the SSZ-type Neotethyan ophiolites in Central Anatolia, Turkey: paleotectonic implications. Geol. J., 35: 53-68.

Yilmaz Y., Serdar H.S. Genc C., Yigitbas E., Gurer F., Elmas A.,Yildirim M., Bozcu M. and Gurpınar O. 1997. The geology and evolution of the Tokat Massif, south central Pontides, Turkey. Intern. Geol. Rev., 39: 365-382.

Received, June 6, 2013
Accepted, September 25, 2013

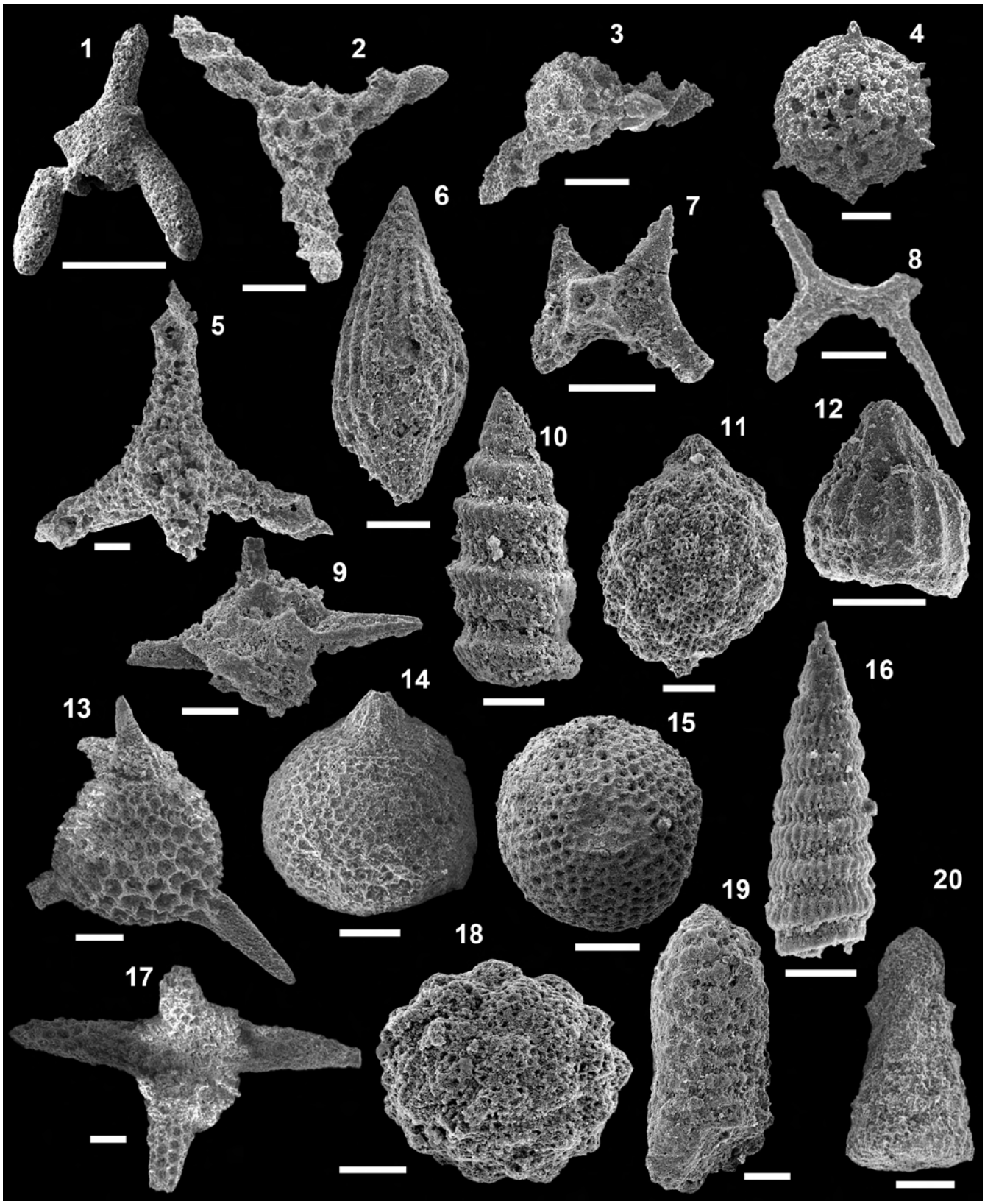


Plate 1 - (scale bar 50$\mu$m) 1) *Ayrtonius elisabethae* Sugiyama, TU10.42; 2) *Betraccium deweveri* Pessagno and Blome, TU10.42; 3) *Betraccium deweveri* Pessagno and Blome, TU10.42; 4) *Braginella rudis* (Bragin), TU10.42; 5) *Tetraporobrachia* sp. A sensu Carter (1993), TU10.42; 6) *Archaeodictyomitra* sp. cf. *A. lacrimula* (Foreman), TU10.31; 7) *Aurisaturnalis carinatus perforatus* Dumitrica and Dumitrica Jud, TU10.31; 8) *Aurisaturnalis variabilis variabilis* (Squinabol), TU10.4; 9) *Cecrops septemporatus* (Parona), TU10.47; 10) *Cinguloturris cylindra* Kemkin & Rudenko, TU10.36; 11) *Cryptamphorella clivosa* (Aliev), TU10.45; 12) *Eucyrtidiellum pyramis* (Aita), TU10.36; 13) *Fultacapsa sphaerica* (Ozvoldova), TU10.28; 14) *Hemicryptocapsa capita* Tan, TU10.4; 15) *Holocryptocanium* sp. cf. *H. barbui* Dumitrica, TU10.45; 16) *Loopus primitivus* (Matsuoka and Yao), TU10.36; 17) *Podocapsa amphitreptera* Foreman, TU10.28; 18) *Praeconosphaera sphaeroconus* (Rüst), TU10.45; 19) *Ristola cretacea* (Baumgartner), TU10.36; 20) *Stichomitra* (?) *takanoensis* Aita, TU10.12.